Accepted Manuscript

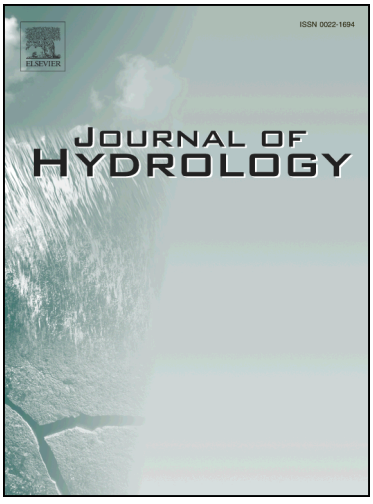

Research papers

Semi-analytical solution of flow to a well in an unconfined-fractured aquifer system separated by an aquitard

Mohammad M. Sedghi, Nozar Samani, D.A. Barry

PII: S0022-1694(18)30179-3
DOI: https://doi.org/10.1016/j.jhydrol.2018.03.012
Reference: HYDROL 22645

To appear in: *Journal of Hydrology*

Received Date: 28 October 2017
Revised Date: 1 March 2018
Accepted Date: 5 March 2018

Please cite this article as: Sedghi, M.M., Samani, N., Barry, D.A., Semi-analytical solution of flow to a well in an unconfined-fractured aquifer system separated by an aquitard, *Journal of Hydrology* (2018), doi: https://doi.org/10.1016/j.jhydrol.2018.03.012

Semi-analytical solution of flow to a well in an unconfined-fractured aquifer system separated by an aquitard

Mohammad M. Sedghi[1,*], Nozar Samani[2], D. A. Barry[3]

[1]Department of Geology, Payame Noor University, Tehran 19395-3697, Iran. m.sedghi@pnu.ac.ir

[2]Department of Earth Science, Shiraz University, Shiraz 71454, Iran. samanin@shirazu.ac.ir

[3]Ecological Engineering Laboratory (ECOL), Environmental Engineering Institute (IIE), Faculty of Architecture, Civil and Environmental Engineering (ENAC), Ecole polytechnique fédérale de Lausanne (EPFL), 1015 Lausanne, Switzerland. andrew.barry@epfl.ch

[*]Corresponding author

A revised manuscript prepared for *Journal of Hydrology*, March 2018

Abstract

Semi-analytical solutions are presented for flow to a well in an extensive homogeneous and anisotropic unconfined-fractured aquifer system separated by an aquitard. The pumping well is of infinitesimal radius and screened in either the overlying unconfined aquifer or the underlying fractured aquifer. An existing linearization method was used to determine the watertable drainage. The solution was obtained via Laplace and Hankel transforms, with results calculated by numerical inversion. The main findings are presented in the form of non-dimensional drawdown-time curves, as well as scaled sensitivity-dimensionless time curves. The new solution permits determination of the influence of fractures, matrix blocks and watertable drainage parameters on the aquifer drawdown. The effect of the aquitard on the drawdown response of the overlying unconfined aquifer and the underlying fractured aquifer was also explored. The results permit estimation of the unconfined and fractured aquifer hydraulic parameters via type-curve matching or coupling of the solution with a parameter estimation code. The solution can also be used to determine aquifer hydraulic properties from an optimal pumping test set up and duration.

Keywords: Three layer-aquifer; Unconfined aquifer; Aquitard; Fractured aquifer; Leakage; Laplace-Hankel transform

Notation

a	Hankel transform parameter
$A_1 - A_3$, $B_1 - B_3$	Coefficients defined in Eqs. (B22)-(B27)
b_1	The overlying unconfined aquifer bottom depth from the initial watertable (L)
b_2	The aquitard bottom depth from the initial watertable (L)
b_3	The underlying fractured aquifer bottom depth from the initial watertable (L)
b_{D2}	Dimensionless initial watertable depth to the aquitard base (defined in Table 1)
b_{D3}	Dimensionless initial watertable depth to the fractured aquifer base (defined in Table 1)
$c_1 - c_6$	Coefficients defined in Eqs. (A37)-(A42) and (B30)-(B35)
d	Vertical distance from the initial watertable to the top of the pumping well screen (L)
d_{D}	Dimensionless depth of the top of the pumping well screen (defined in Table 1)
K_{m}	Hydraulic conductivity of the matrix blocks (LT^{-1})
K_{ra}	Horizontal hydraulic conductivity of the aquitard (LT^{-1})
K_{rf}	Horizontal hydraulic conductivity of the fractured aquifer (LT^{-1})

K_{ru}	Horizontal hydraulic conductivity of the unconfined aquifer (LT^{-1})
K_{za}	Vertical hydraulic conductivity of the aquitard (LT^{-1})
K_{zf}	Vertical hydraulic conductivity of the fractured aquifer (LT^{-1})
K_{zu}	Vertical hydraulic conductivity of the unconfined aquifer (LT^{-1})
l	Vertical distance from the initial watertable to the bottom of the pumping well screen (L)
l_{D}	Dimensionless depth of the bottom of the pumping well screen (defined in Table 1)
p	Lapalce transform parameter
Q	Pumping well flux (L^3T^{-1})
$\tilde{r}_{\mathrm{m}}$	Radius of matrix blocks (L)
$\tilde{r}$	Radial distance from the center of matrix blocks (L)
r	Radial distance from the pumping well (L)
r_{D}	Dimensionless distance from the pumping well (defined in Table 1)
s_{a}	Drawdown in the aquitard (L)
s_{f}	Drawdown in the fractured aquifer (L)
s_{u}	Drawdown in the unconfined aquifer (L)

$\hat{\bar{s}}_{\mathrm{aD}}$	Laplace-Hankel domain dimensionless drawdown in aquitard
$\hat{\bar{s}}_{\mathrm{fD}}$	Laplace-Hankel domain dimensionless drawdown in fractured aquifer
$\hat{\bar{s}}_{\mathrm{uD}}$	Laplace-Hankel domain dimensionless drawdown in the unconfined aquifer
$\bar{s}_{\mathrm{aD}}$	Laplace domain dimensionless drawdown in the aquitard
$\bar{s}_{\mathrm{fD}}$	Laplace domain dimensionless drawdown in the fractured aquifer
$\bar{s}_{\mathrm{uD}}$	Laplace domain dimensionless drawdown in the unconfined aquifer
S_{sa}	Specific storage of the aquitard (L^{-1})
S_{sf}	Specific storage of the fractured aquifer (L^{-1})
S_{su}	Specific storage of the unconfined aquifer (L^{-1})
S_{y}	Specific yield of the unconfined aquifer
t	Time from start of pumping (T)
t_{D}	Dimensionless time from the start of pumping (defined in Table 1)
z	Vertical distance from the initial watertable (L)
z_{D}	Dimensionless vertical distance from the initial watertable (defined in Table 1)
$w_{\mathrm{D1}}, w_{\mathrm{D2}}$	Coefficients defined in Eqs. (B28) and (B29)
α_{ra}	Horizontal hydraulic diffusivity of the aquitard defined as $\frac{K_{\mathrm{ra}}}{S_{\mathrm{sa}}}$ (L^2T^{-1})

α_{rf}	Horizontal hydraulic diffusivity of the underlying fractured aquifer defined as $\frac{K_{\mathrm{rf}}}{S_{\mathrm{sf}}}$ (L^2T^{-1})
α_{ru}	Horizontal hydraulic diffusivity of the overlying unconfined aquifer defined as $\frac{K_{\mathrm{ru}}}{S_{\mathrm{su}}}$ (L^2T^{-1})
α_{za}	Vertical hydraulic diffusivity of the aquitard defined as $\frac{K_{\mathrm{za}}}{S_{\mathrm{sa}}}$ (L^2T^{-1})
α_{zf}	Vertical hydraulic diffusivity of the underlying fractured aquifer defined as $\frac{K_{\mathrm{zf}}}{S_{\mathrm{sf}}}$ (L^2T^{-1})
α_{zu}	Vertical hydraulic diffusivity of the overlying unconfined aquifer defined as $\frac{K_{\mathrm{zu}}}{S_{\mathrm{su}}}$ (L^2T^{-1})
$\alpha_{\mathrm{Dr}}^{\mathrm{a}}$	Dimensionless term introduced in Eq. (A2) (defined in Table 1)
$\alpha_{\mathrm{Dr}}^{\mathrm{f}}$	Dimensionless term introduced in Eq. (A3) (defined in Table 1)
$\alpha_{\mathrm{Dz}}^{\mathrm{a}}$	Dimensionless term introduced in Eq. (A2) (defined in Table 1)
$\alpha_{\mathrm{Dz}}^{\mathrm{f}}$	Dimensionless term introduced in Eq. (A3) (defined in Table 1)
$\alpha_{\mathrm{Dz}}^{\mathrm{u}}$	Dimensionless term introduced in Eq. (A1) (defined in Table 1)
α_{y}	Parameter associated with watertable drainage defined as $\frac{b_1 K_{zu}}{S_y}$ (L^2T^{-1})
β	Linearization parameter appears in Eq. (16) (L)
β_{D}	Dimensionless parameter introduced in Eq. (A10) (defined in Table 1)

Γ_{m}	Inter-porosity flux term, see Eqs. (3) and (4)
γ_1	Dimensionless parameter introduced in Eq. (A28) (defined in Table 1)
γ_2	Dimensionless parameter introduced in Eq. (A32) (defined in Table 1)
η_{a}	Dimensionless parameter introduced in Eq. (A26) (defined in Table 1)
η_{f}	Dimensionless parameter introduced in Eq. (A30) (defined in Table 1)
η_{u}	Dimensionless parameter introduced in Eq. (A21) (defined in Table 1)
θ_1, θ_2, χ	Coefficients defined in Eqs. (A43-A45) and (B36)
ϑ	Coefficients defined in Eq. (A56)
ψ_1, ψ_4	Coefficients defined in Eqs. (A46)-(A49)
ξ	Dimensionless parameter introduced in Eq. (A10) (defined in Table 1)
σ	Coefficients defined in Eq. (A57)

1. Introduction

We consider unconfined aquifers that are hydraulically connected to underlying fractured aquifers, examples of which are found in different parts of the world (Al-Shaibani, 2008; Milanovic and Aghili, 1993; Sedghi and Samani, 2015; Subyani, 2004; Wagner, 2011). Often, an aquitard separates the unconfined aquifer from the underlying fractured aquifer. For example, in the Zagros Mountains (southwest Iran), clay and marl layers separate the underlying fractured limestone aquifer from the overlying alluvial layers (Issar, 1969). Similarly, the aquifer-aquitard

system in the Waterloo Moraine (Ontario, Canada) is underlain by a limestone aquifer (Martin and Frind, 1998). An aquifer system in the southern Syrian steppe contains Upper Cretaceous and Paleogene limestone and chalk aquifers that are, in some areas, separated by a marly aquitard (Wagner, 2011). Available mathematical models describing leaky and multilayer aquifer systems are not suitable to describe the above-mentioned aquifer systems. For that reason, here we develop an analytical model of flow to a well in unconfined-fractured aquifer system separated by an aquitard.

There are several analytical solutions for flow to a well in leaky and multilayer aquifer systems. The solutions of Hantush and Jacob (1955) and Hantush (1967) do not consider aquifer storage. Instead, the aquitard transmits water from a constant head source to the aquifer. Hantush (1960), Neuman and Witherspoon (1969), Moench (1985) and Zhan and Park (2003) take account of the storativity of the aquitard but impose leakage over the whole aquifer thickness. The more realistic condition in which the leakage is imposed through the aquifer-aquitard boundary was presented by Hunt (2005), Sun and Zhan (2006) and Sedghi et al. (2012). An aquitard separating two aquifer layers was considered by Malama et al. (2008). A generalized matrix-form solution for a coupled multilayer aquifer system was derived by Veling and Maas (2009). The inter-porosity flow of the underlying fractured aquifer and the second derivative of the watertable condition can be applied to their solutions. However, Veling and Maas (2009) did not formulate the closed form expression for their solution in the *z* direction.

The free surface boundary condition requires some care in aquifer modeling. The instantaneous drainage model of Neuman (1972, 1974) was employed in many models (Malama et al., 2007, 2008; Samani and Sedghi, 2015; Sedghi and Samani, 2015). The alternative of gradual watertable drainage was presented by Moench (1995, 1996, 1997) and adopted in the solutions of

Zhan and Zlotnik (2002) and Sedghi et al. (2009). Tartakovsky and Neuman (2007) presented an analytical solution for the delayed watertable response (due to the unsaturated flow above the watertable) to pumping from a partially penetrating well. Their solution was extended by Mishra and Neuman (2010) to the case of an unsaturated zone of finite thickness. The method presented by Mishra and Neuman (2010) was also used by Mishra et al. (2012) to obtain an analytical solution for flow to a vertical well in a leaky-unconfined aquifer. The coupled unsaturated-saturated flow is also considered by Liang et al. (2017a) to model the drawdown induced by horizontal, vertical and slanted wells in unconfined aquifer. The unsaturated zone thickness, among other factors, also affects the specific yield as stated by Liang et al. (2017b) referring to Parlange and Brutsaert (1987). When applied to data from the glacial out-wash aquifer in Cape Cod reported by Moench et al. (2000), the models of Neuman (1972, 1974), Moench (1995, 1996, 1997) and Tartakovsky and Neuman (2007) failed to achieve reasonable estimates of the specific yield (Malama, 2011). Malama (2011) presented a new analytical solution for flow to a well in an unconfined aquifer using an alternative linearization of the nonlinear kinematic condition at the watertable. This solution significantly improved the estimation of specific yield from the pumping test data. In this work, the method suggested by Malama (2011) is adapted to simulate the watertable boundary condition.

Modeling of fractured aquifers and reservoirs is a long-standing research topic. The dual porosity concept presented by Barenblatt et al. (1960) is often used to describe fractured aquifer/reservoir hydraulics/dynamics (Bourdet and Gringarten, 1980; Gringarten et al., 1981; Deruyck et al., 1982; Park and Zhan, 2003; Sedghi and Samani, 2010; Sedghi and Samani, 2015). For example, Warren and Root (1963) used steady state inter-porosity flow to characterize the behavior of naturally fractured reservoirs. Their single-phase flow solution was extended to two-phase flow

by Kazemi et al. (1976) using a numerical method. Duguid and Lee (1977) used a finite element method to simulate transient inter-porosity flow. Both constant discharge and step drawdown problems are considered in their work. Drawdown equations for flow in fissures – whether voids or filled with fine materials – and porous flow due to discharge from a pumping well were obtained by Streltsova (1976). For a specific heterogeneous formation, he obtained the drawdown equation for an aquifer-aquitard system. An unconfined fractured aquifer was considered using the double-porosity concept by Boulton and Streltsova (1977). Bourdet and Gringarten (1980) and Gringarten et al. (1981) presented a method of determining block size and fissure volumes using type-curve matching. Deruyck et al. (1982) obtained Laplace-domain inter-porosity flow equations for both spherical and slab-shaped matrix blocks. Transient inter-porosity flow and rectangular-shaped matrix blocks were considered by Serra et al. (1983). The double porosity approach can be used to simulate flow in karstified limestone, as shown by Sauter (1990) using field data.

In the following, we present a semi-analytical solution for flow to a partially penetrating pumping well in an unconfined-fractured aquifer system separated by an aquitard. The pumped well is screened in either the overlying unconfined aquifer or the underlying fractured aquifer. The dual porosity concept presented by Barenblatt et al. (1960) is adopted to simulate the inter-porosity flow in the fractured aquifer. The results are presented in the form of dimensionless drawdown and scaled sensitivity curves.

2. Method

2.1. Conceptual model

Figure 1 shows the three-dimensional conceptual model of an unconfined-fractured aquifer system separated by an aquitard with a partially penetrating pumping well and a piezometer. The origin of the coordinate system (r, z) is located at the intersection of the pumping well centerline and the initial watertable position, while the z-axis is positive upward. The pumping well is screened from depth d to l measured from the watertable. The aquitard extends from depth b_1 to b_2. The underlying fractured aquifer extends from the bottom of aquitard to depth b_3. The overlying unconfined aquifer, the aquitard and the underlying fractured aquifer are (individually) homogeneous and anisotropic with uniform thickness and infinite radial extent. The watertable decline due to pumping is assumed to be negligible compared to the aquifer thickness. The base of the fractured aquifer is a no-flow boundary.

The governing equations for two-dimensional transient drawdown are (Malama et al., 2007):

$$\frac{K_{\mathrm{ru}}}{r}\frac{\partial}{\partial r}\left(r\frac{\partial s_{\mathrm{u}}}{\partial r}\right)+K_{\mathrm{zu}}\frac{\partial^2 s_{\mathrm{u}}}{\partial z^2}=S_{\mathrm{su}}\frac{\partial s_{\mathrm{u}}}{\partial t} \qquad (1)$$

for the overlying unconfined aquifer,

$$\frac{K_{\mathrm{ra}}}{r}\frac{\partial}{\partial r}\left(r\frac{\partial s_{\mathrm{a}}}{\partial r}\right)+K_{\mathrm{za}}\frac{\partial^2 s_{\mathrm{a}}}{\partial z^2}=S_{\mathrm{sa}}\frac{\partial s_{\mathrm{a}}}{\partial t} \qquad (2)$$

for the aquitard and,

$$\frac{K_{\mathrm{rf}}}{r}\frac{\partial}{\partial r}\left(r\frac{\partial s_{\mathrm{f}}}{\partial r}\right)+K_{\mathrm{zf}}\frac{\partial^2 s_{\mathrm{f}}}{\partial z^2}+\Gamma_{\mathrm{m}}=S_{\mathrm{sf}}\frac{\partial s_{\mathrm{f}}}{\partial t} \qquad (3)$$

for the underlying fractured aquifer, where s_{u}, s_{a} and s_{f} are drawdown (m); K_{ru}, K_{ra} and K_{rf} are the horizontal hydraulic conductivities (ms^{-1}); K_{zu}, K_{za} and K_{zf} are the vertical hydraulic

conductivities (ms^{-1}); S_{su}, S_{sa} and S_{sf} are the specific storages (m^{-1}), the subscripts u, a and f represent the unconfined aquifer, the aquitard and the fractured aquifer, respectively, and Γ_m is the inter-porosity flow term (s^{-1}) defined as (Deruyck et al., 1982; Park and Zhan, 2003):

$$\Gamma_m = \frac{3K_m}{\tilde{r}_m}\frac{\partial s_m}{\partial \tilde{r}}\bigg|_{\tilde{r}=\tilde{r}_m} \quad (4)$$

The interfracture material is conceptualized as spherical blocks, so s_m, which is the drawdown in the matrix blocks (m), is defined by (Deruyck et al., 1982):

$$\frac{K_m}{\tilde{r}^2}\frac{\partial}{\partial \tilde{r}}\left(\tilde{r}^2\frac{\partial s_m}{\partial \tilde{r}}\right) = S_{sm}\frac{\partial s_m}{\partial t} \quad (5)$$

where K_m is the matrix block hydraulic conductivity (ms^{-1}); $\tilde{r}$ is the radial distance from the center of the spherical matrix blocks (m); $\tilde{r}_m$ is the radius of matrix blocks (m) and S_{sm} is the specific storage of the matrix blocks (m^{-1}). The initial and boundary conditions for the matrix blocks are, respectively:

$$s_m(\tilde{r},0) = 0 \quad (6)$$

$$\lim_{\tilde{r}\to\tilde{r}_m} s_m(\tilde{r},t) = s_f(r,z,t) \quad (7)$$

It should be noted that Eq. (7) is wrongly presented in Sedghi and Samani (2015, Eq. 11).

The watertable before pumping is horizontal, so the initial condition is:

$$s_u(r,z,0) = s_a(r,z,0) = s_f(r,z,0) \quad (8)$$

As the aquifer system is considered to be extensive, the far-field boundary condition is:

$$\lim_{r\to\infty} s_u(r,z,t) = \lim_{r\to\infty} s_a(r,z,t) = \lim_{r\to\infty} s_f(r,z,t) = 0 \quad (9)$$

If the pumping well is screened in the overlying unconfined aquifer (conceptual Model I, Fig. 1a), the boundary conditions at the pumping well are (Malama et al., 2007, 2008; Sedghi and Samani, 2015):

$$\lim_{r\to 0} r\frac{\partial s_{\mathrm{u}}}{\partial r} = \begin{cases} 0 & -d < z < 0 \\ -\dfrac{Q}{2\pi K_{\mathrm{ru}}(l-d)} & -l < z < -d \\ 0 & -b_1 < z < -l \end{cases} \tag{10}$$

$$\lim_{r\to 0} r\frac{\partial s_{\mathrm{a}}}{\partial r} = 0 \tag{11}$$

$$\lim_{r\to 0} r\frac{\partial s_{\mathrm{f}}}{\partial r} = 0 \tag{12}$$

The conditions for the corresponding case in which the well is screened in the underlying fractured aquifer are (conceptual Model II, Fig. 1b):

$$\lim_{r\to 0} r\frac{\partial s_{\mathrm{f}}}{\partial r} = \begin{cases} 0 & -d < z < -b_2 \\ -\dfrac{Q}{2\pi K_{\mathrm{rf}}(l-d)} & -l < z < -d \\ 0 & -b_3 < z < -l \end{cases} \tag{13}$$

$$\lim_{r\to 0} r\frac{\partial s_{\mathrm{u}}}{\partial r} = 0 \tag{14}$$

$$\lim_{r\to 0} r\frac{\partial s_{\mathrm{a}}}{\partial r} = 0 \tag{15}$$

The linearization method of Malama (2011) is adopted to model the watertable drainage:

$$K_{\mathrm{zu}}\left(\left.\frac{\partial s_{\mathrm{u}}}{\partial z}\right|_{z=0} + \beta\left.\frac{\partial^2 s_{\mathrm{u}}}{\partial z^2}\right|_{z=0}\right) + S_{\mathrm{y}}\left.\frac{\partial s_{\mathrm{u}}}{\partial t}\right|_{z=0} = 0 \tag{16}$$

where β (m) is a linearization parameter and S_{y} is the specific yield of the unconfined aquifer. The no-flow condition is applied at the base of the fractured aquifer:

$$\left.\frac{\partial s_{\mathrm{f}}}{\partial z}\right|_{z=-b_3} = 0 \tag{17}$$

Drawdown and flux are each conserved across the interface of the unconfined aquifer and the aquitard:

$$s_{\mathrm{u}}(r,-b_1,t) \;=\; s_{\mathrm{a}}(r,-b_1,t) \tag{18}$$

$$K_{\mathrm{zu}}\frac{\partial s_{\mathrm{u}}}{\partial z}\bigg|_{z\,=\,-b_1} \;=\; K_{\mathrm{za}}\frac{\partial s_{\mathrm{a}}}{\partial z}\bigg|_{z\,=\,-b_1} \tag{19}$$

as well as across the aquitard-fractured aquifer interface:

$$s_{\mathrm{a}}(r,-b_2,t) \;=\; s_{\mathrm{f}}(r,-b_2,t) \tag{20}$$

$$K_{\mathrm{za}}\frac{\partial s_{\mathrm{a}}}{\partial z}\bigg|_{z\,=\,-b_2} \;=\; K_{\mathrm{zf}}\frac{\partial s_{\mathrm{f}}}{\partial z}\bigg|_{z\,=\,-b_2} \tag{21}$$

Solving Eqs. (1-3) subject to initial and boundary conditions of Eqs. (4-21) for the case in which the pumping well is screened in the overlying unconfined aquifer (Fig. 1a, Model I) results in the following dimensionless drawdown equations (Appendixes A and B) for the unconfined aquifer, aquitard and fractured aquifer, respectively:

$$\bar{s}_{\mathrm{uD}} \;=\; \int_0^\infty a[\hat{u}_{\mathrm{D}} + c_1\exp(\eta_{\mathrm{u}}z_{\mathrm{D}}) + c_2\exp(-\eta_{\mathrm{u}}z_{\mathrm{D}})]\,\mathrm{J}_0(ar_{\mathrm{D}})da \tag{22}$$

$$\bar{s}_{\mathrm{aD}} \;=\; \int_0^\infty a[c_3\exp(\eta_{\mathrm{a}}z_{\mathrm{D}}) + c_4\exp(-\eta_{\mathrm{a}}z_{\mathrm{D}})]\,\mathrm{J}_0(ar_{\mathrm{D}})da \tag{23}$$

$$\bar{s}_{\mathrm{fD}} \;=\; \int_0^\infty a[c_5\exp(\eta_{\mathrm{f}}z_{\mathrm{D}}) + c_6\exp(-\eta_{\mathrm{f}}z_{\mathrm{D}})]\,\mathrm{J}_0(ar_{\mathrm{D}})da \tag{24}$$

where the parameters appearing in Eqs. (22-24) are defined in Appendix A.

For the case in which the pumping well is screened in the underlying fractured aquifer (Fig. 1b, Model II), the solutions corresponding to Eqs. (22-24) for the dimensionless drawdown are, respectively:

$$\bar{s}_{\mathrm{uD}} \;=\; \int_0^\infty a[c_1\exp(\eta_{\mathrm{u}}z_{\mathrm{D}}) + c_2\exp(-\eta_{\mathrm{u}}z_{\mathrm{D}})]\,\mathrm{J}_0(ar_{\mathrm{D}})da \tag{25}$$

$$\bar{s}_{\mathrm{aD}} = \int_0^\infty a[c_3\exp(\eta_{\mathrm{a}} z_{\mathrm{D}}) + c_4\exp(-\eta_{\mathrm{a}} z_{\mathrm{D}})]\,\mathrm{J}_0(ar_{\mathrm{D}})da \qquad (26)$$

$$\bar{s}_{\mathrm{fD}} = \int_0^\infty a[\hat{u}_{\mathrm{D}} + c_5\exp(\eta_{\mathrm{f}} z_{\mathrm{D}}) + c_6\exp(-\eta_{\mathrm{f}} z_{\mathrm{D}})]\,\mathrm{J}_0(ar_{\mathrm{D}})da \qquad (27)$$

where parameters appearing in Eqs. (25-27) are defined in Appendix B.

3. Results and Discussion

In this section, the time-drawdown responses of the three-layer aquifer system are investigated by generating the dimensionless drawdown-time type curves. The dimensionless drawdown data are obtained via numerical inverse Laplace (De Hoog et al., 1982) and Hankel (Michels, 1963; Press et al., 1992) transforms following the method outlined by Sedghi and Samani (2015). Type curves for conceptual Model I and Model II (Fig. 1) are generated using Eqs. (22-24) and Eqs. (25-27), respectively. The default dimensionless parameter ratios given in Table 2 are used to construct the type curves. The type curves presented in this section are compared with Neuman's type curve for unconfined aquifers (Neuman, 1974) and the Malama et al. (2008) type curves for the aquifer-aquitard system. This comparison permits examination of the effects of the underlying fractured aquifer on the dimensionless drawdown in the three-layer aquifer system.

Scaled sensitivity-dimensionless time curves are also presented below. Using these curves, the effects of the aquitard hydraulic parameters on the sensitivity of the overlying unconfined aquifer dimensionless drawdown to the underlying fractured aquifer parameters are explored.

3.1 Drawdown response of the three-layer aquifer system due to pumping the overlying unconfined aquifer (Model I, Fig. 1a)

The dimensionless drawdown response of the three-layer aquifer system is investigated in this section. Three piezometer points are considered. The first is in the overlying unconfined aquifer at the depth of z_D = -0.5, the second is in the aquitard at the depth of z_D = -1.2 and the third is in the underlying fractured aquifer at the depth of z_D = -2.0. The pumping well is screened in the unconfined aquifer. Responses at these three z_D locations for different conditions will be examined in the following.

Figure 2 shows that the dimensionless drawdowns in the overlying unconfined aquifer (black curves, z_D = -0.5) follow the Neuman unconfined aquifer type curve at early times (t_D < 0.1) before being affected by the underlying fractured aquifer. It then deviates somewhat from Neuman's curve at intermediate times (0.1 < t_D < 10). This occurs because the fractured aquifer feeds the unconfined aquifer via the aquitard, which reduces the drawdown in the unconfined aquifer and thus deviates from Neuman's curve. The deviation increases proportionally to the value of K_{rf}/K_{ru} during at late times (t_D > 5000) due to increased leakage from the underlying aquitard and fractured aquifer, which results from the potential head difference established between the pumped unconfined aquifer and the fractured aquifer.

The aquitard responds to the pumped well in the unconfined aquifer. The dimensionless drawdowns in the aquitard (Fig. 2, blue curves, z_D = -1.2) due to the pumped well starts at time t_D = 5, which is two orders of magnitude later than in the unconfined aquifer (i.e., results for z_D = -0.5). While during the late time stage the drawdown curves diverge in proportion to the K_{rf}/K_{ru} values, the effect of hydraulic conductivity ratios is obscured at early and intermediate times, up

to about $t_D = 10^4$ (i.e., blue curves overlie each other). In all times, the drawdown values in the aquitard ($z_D = -1.2$) are less than those of the unconfined aquifer ($z_D = -0.5$), as expected.

The fractured aquifer also responds to the pumped well in the unconfined aquifer. The dimensionless drawdowns in the fractured aquifer (Fig. 2, red curves, $z_D = -2.0$) due to the pumped well are significantly different and less than those in the unconfined aquifer and the aquitard. The effect of K_{rf}/K_{ru} on the dimensionless drawdown in the fractured aquifer is significant and is readily apparent from early to late time.

The three sets of drawdown curves in Fig. 2 provide guidance on the determination of parameters in such aquifers. Given the large differences in the drawdowns depicted in Fig. 2, estimation of physical parameters characterizing water-bearing layers in the unconfined-aquitard-fractured aquifer system should be based on the data collected from piezometers installed in each individual layer. In addition, Fig. 2 reveals that the curves based on the solution of Malama et al. (2008) at $z_D = -2.0$ deviate from the proposed solution during the early and intermediate times. This difference is due to the release of stored water in the interfracture matrix, which reduces drawdown in the fractured aquifer. By contrast, drawdown curves from the solution of Malama et al. (2008) agree closely with those from the new solution in the overlying unconfined aquifer and the aquitard as the effects of interporosity flow diminished in the overlying unconfined aquifer and the aquitard (curves not shown).

Figure 3, in a manner similar to Fig. 2, shows the effects of the vertical hydraulic conductivity of the fractured aquifer. Three measurement locations are considered, using the ratio of vertical hydraulic conductivities, K_{zf}/K_{zu}, as a parameter. As the fractured aquifer is underlain by an impermeable layer and overlain by an aquitard, the effect of the vertical component of flow on

the overlying unconfined aquifer is negligible, i.e., the dimensionless drawdown in the unconfined aquifer is not sensitive to K_{zf}/K_{zu}. However, the presence of the underlying aquitard and fractured aquifer causes the unconfined aquifer response to deviate from that of Neuman's (1974) solution. Moreover, the inter-porosity flow modifies the type curves for the underlying fractured aquifer from that of Malama et al. (2008) during early times. These differences are not observed in the overlying unconfined aquifer and the aquitard (curves not shown). In essence, the effects of inter-porosity flow are not significant for the aquitard and for the overlying unconfined aquifer.

We next considered the effect of the hydraulic conductivity (K_m) of the interfracture matrix blocks. Figure 4 shows results at the three z_D observation locations for varying K_{rf}/K_m and using default parameter ratios of Table 2. The dimensionless drawdowns are compared with the model presented by Malama et al. (2008). As seen in Fig. 4, the effect of K_m is negligible in the overlying unconfined aquifer and the aquitard (black and blue curves). The inter-porosity flow, however, affects the dimensionless drawdown in the underlying fractured aquifer leading to differences between the presented solution from that of Malama et al. (2008) during the early and intermediate times when the inter-porosity flow dominates. As expected, the new solution also shows differences to results from the solution of Neuman (1974) due to the release of water stored in the aquitard and underlying fractured aquifer.

In Fig. 5, the effect of specific storage of the matrix blocks on dimensionless drawdown is displayed. As in Fig. 4, the dimensionless drawdowns are compared with the Malama et al. (2008) solution. Drawdown in the unconfined aquifer and the aquitard is similar for both solutions. However, increasing S_{sm} reduces the dimensionless drawdown in the fractured aquifer

as more water is released from the matrix blocks, causing results to differ for the underlying fractured aquifer.

The specific yield (S_y) of the overlying unconfined aquifer affects the dimensionless drawdown in the aquifer system (Fig. 6). Specifically, increasing S_y decreases the intermediate and late time dimensionless drawdown in all three layers. The role of S_y is apparent in its specification in the boundary condition at the watertable (Malama, 2011):

$$S_y \frac{\partial h}{\partial t} = -K_z \frac{\partial h}{\partial z} + \mathbf{K}\nabla h \cdot \nabla h \qquad (28)$$

where $\mathbf{K}$ is the aquifer conductivity tensor. Equation 28 is simplified to (Malama, 2011):

$$S_y \frac{\partial h}{\partial t} = -K_z \left(\frac{\partial h}{\partial z} + h \frac{\partial^2 h}{\partial z^2} \right) \qquad (29)$$

To linearize the above equation the variable h at the second right hand side term of Eq. (29) is replaced by a constant β to yield Eq. (16) (Malama, 2011). This constant, in its dimensionless form, β_D (Table 1), ranges from 0 to 1. For the case in which $\beta_D = 0$ (practically for β_D lower than 0.1 as shown in Fig. 7), the diffuse watertable boundary condition (Eq. 16) reduces to the sharp interface condition (Neuman, 1972, 1974), i.e., varying β_D changes the interface from sharp to diffuse. This, on the other hand, violate the underlying assumption of the instantaneous water table drainage model (Neuman, 1972) in which the drawdown is negligible comparing to the aquifer thickness (i.e. $\beta_D \cong 1$). Therefore the difference between the dimensionless drawdown curves prepared for $\beta_D = 1$ and $\beta_D = 0$ reveals the error resulting from Dagan (1967) linearization adapted by Neuman (1972, 1974). Clearly, both β_D and the specific yield, S_y, affect release of water from the watertable (Malama, 2011). The effects of varying β_D are explored in Fig. 7. As illustrated in the figure, increasing β_D decreases the intermediate and late time drawdown in the three-layer aquifer system. It is evident that increasing β_D increases the

watertable drainage (Eq. 29). Thus, the drawdown decreases during the intermediate and late times. As noted by Malama (2011), the sensitivity of the late time dimensionless drawdown to β_D for fixed S_y explains why the diffuse interface watertable model improves estimation of S_y. Since β_D affects the late time dimensionless drawdown in the all three layers, using the diffuse interface watertable condition improves the estimate of S_y using the drawdown data collected from each aquifer layer. More importantly, the diffuse interface condition is more realistic than the sharp interface (Malama, 2011).

3.2 Drawdown response of the three-layer aquifer system due to pumping the underlying fractured aquifer (Model II, Fig. 1b)

In this section, the effects of pumping the underlying fractured aquifer on the dimensionless drawdown response of water-bearing layers in the unconfined-aquitard-fractured aquifer system are investigated and compared with those of Model I. Figure 8 is first constructed for different K_{rf}/K_{ru} values. The pumping well is screened in the underlying fractured aquifer (d_D = 2 and l_D = 2.5, with other parameters are set to values as listed in Fig. 2). Inspection of Fig. 8 reveals that both the overlying aquifer and aquitard respond to the pumped well in the fractured aquifer. The drawdown in the aquitard and in the unconfined aquifer is always less than that of the fractured aquifer, as expected. The drawdown in the three-layer aquifer system is inversely proportional to the K_{rf}/K_{ru} ratio. Furthermore, comparing Figs. 2 and 8 shows that the dimensionless drawdown is more sensitive to K_{rf}/K_{ru} for Model II (well is screened in the underlying fractured aquifer) than Model I (well is screened in the overlying aquifer).

The effect of the vertical hydraulic conductivity of the fractures on the dimensionless drawdown in the aquifer system is not major in the case of the Model II (i.e., the pumping well is screened in the underlying fractured aquifer (d_D = 2, l_D = 2.5, Fig. 9)) compared to Model I (Fig. 3). In other words, the vertical flow component in the fractured aquifer is not significant enough to affect the overlying aquifers in contrast to the horizontal flow component (Fig. 8).

In Fig. 10, we observed that the value of K_m (interfracture hydraulic conductivity) affects the dimensionless drawdown in the aquifer system of Model II in the same manner as in Model I (Fig. 4). Figure 10 shows that increasing the hydraulic conductivity of the matrix blocks reduces the early time dimensionless drawdown in the underlying fractured aquifer. The same phenomenon was reported by Park and Zhan (2003) and Sedghi and Samani (2015). This effect is more pronounced compared to Model I (Fig. 4). The dimensionless drawdown in the overlying unconfined aquifer and the aquitard is not sensitive to K_m (Fig. 10, blue and black curves).

The specific yield, S_y, affects the dimensionless drawdown in the Model II aquifer system, as shown in Fig. 11. Comparing Figs. 6 (Model I) and 11 (Model II) reveals that, in both models, increasing S_y decreases the intermediate and late time dimensionless drawdowns, although in Model II the dimensionless drawdown is more sensitive.

In the case that the pumping well is screened in the underlying fractured aquifer, the influence of the specific storage of the matrix blocks, S_{sm}/S_{sf}, is more significant (Fig. 12) compared to the case where the pumping well is screened in the overlying unconfined aquifer (Fig. 5). Furthermore, the storativity of matrix affects the dimensionless drawdown in all three layers of aquifer system (Fig. 12).

The effects of linearization parameter β_{D} are explored for the case in which the pumping well is screened in the underlying fractured aquifer (Fig. 13). As illustrated in Fig. 13, the influence of β_{D} is less marked in this case (Model II) than in Model I (Fig. 7) owing to the fact that the contribution of the watertable drainage to the pumped well is low as the pumping well screened in the underlying fractured aquifer.

3.3 The role of aquitard on the water transfer between the upper and lower aquifers

To investigate the transfer of water from the underlying fractured aquifer to the overlying aquifer through the aquitard, scaled sensitivity curves are plotted. Scaled sensitivity is calculated using (Huang and Yeh, 2007):

$$S_{pi} = P_i \frac{O(P_i + \Delta P_i) - O(P_i)}{\Delta P_i} \qquad (30)$$

where S_{pi} is the scaled sensitivity; P_i is the aquitard parameter (e.g., S_{sa}); O is the response of the overlying aquifer (e.g., $\bar{s}_{\mathrm{uD}}$) and ΔP_i is the relative parameter increment, which in the following is calculated as $\Delta P_i = 10^{-3} P_i$ (Huang and Yeh, 2007). The sensitivity plots are reported in the Supplementary Material. The results indicate that increases in the vertical hydraulic conductivity, K_{za}, and decreases in the specific storage, S_{sa}, and the thickness of the aquitard increase the leakage from the underlying fractured aquifer to the overlying unconfined aquifer (see the Supplementary Material). This affects the dimensionless drawdown in the overlying unconfined aquifer. Therefore, the three-layer model proposed here is necessary where thin aquitards with high vertical hydraulic diffusivities, α_{za}, ($\alpha_{\mathrm{za}}/\alpha_{\mathrm{zu}}$ greater than about 4×10^{-7}) are located between the overlying unconfined and the underlying fractured aquifers.

Interestingly, the effects of horizontal hydraulic conductivity of the aquitard, K_{ra}, on the leakage from the underlying fractured aquifer to the overlying unconfined aquifer is negligible as it does not affect the vertical flow in the aquitard.

4. Aquifer parameter estimation

The presented solution can be used to obtain aquifers hydraulic parameters by the means of coupling with a parameter estimation code e.g. PEST (Doherty et al., 1994).

Using a pumping well screened in the overlying unconfined aquifer and a piezometer installed in the underlying fractured aquifer one can estimate aquifer system hydraulic parameters except the hydraulic conductivity of the matrix blocks (K_m) (Figures 2-6). If one were to estimate K_m using the pumping test data, the pumping well must screen in the underlying fractured aquifer and the piezometer must be installed there. Interestingly, the vertical hydraulic conductivity of fractures (K_{zf}) cannot be estimated using this configuration as the vertical component of flow is negligible. In this case the first mention configuration must be used (Figs.3 and 9).

To estimate the specific yield, the linearization parameter should not be frozen during the parameter estimation. This improves the estimation of S_y. For more information on the range of linearization parameter the readers may consult Malama (2011).

5. Conclusions

The Laplace-Hankel domain solution of the flow to a partially penetrating pumping well in a homogeneous, anisotropic and laterally infinite unconfined-fractured aquifer system separated by an aquitard is obtained. Two conceptual models are considered. In Model I, the pumping well is screened in the overlying unconfined aquifer and in Model II the pumping well is screened in the

underlying fractured aquifer. The linearization method suggested by Malama (2011) is used to simulate the watertable drainage. The double porosity approach (Barenblatt et al., 1960) is adapted to simulate the inter-porosity flow between the spherical matrix blocks and the fracture network in the underlying fractured aquifer (Deruyck et al., 1982). The time domain drawdown data are calculated using the De Hoog et al. (1982) numerical Laplace inversion and Gaussian quadrature (Michels, 1963; Press et al., 1992) and presented in the form of dimensionless drawdown type curves. The type curves of Model I are compared with those of single layer-unconfined aquifer and double-layer aquifer-aquitard systems. The drawdown behavior of the three-layer aquifer system in response to pumping of the overlying unconfined aquifer and the underlying fractured aquifer are investigated. The effect of hydraulic parameter variations of each individual layer on the response of the three-layer aquifer system is also explored. The results lead to the following conclusions:

- In Model I, the three layers respond to the pumping well and the drawdown is inversely proportional to the horizontal hydraulic conductivity ratio (K_{rf}/K_{ru}). The response of the overlying unconfined aquifer deviates from the Neuman solution (in which the watertable is considered as a sharp interface) at intermediate and late times due to the linearization parameter (β_D) (which affects the release of water from the watertable), and the presence of the underlying fractured aquifer and aquitard. In contrast, the drawdown in all the three layers is quite insensitive to the vertical hydraulic conductivity of the underlying fractured aquifer (K_z). The effect of the hydraulic conductivity and the specific storage of the matrix blocks of the underlying fractured aquifer (K_m, S_{sm}) is negligible on the overlying unconfined aquifer and the aquitard response as the influence of the inter-porosity flow is significantly diminished there. However, it affects the dimensionless drawdown in the underlying fractured

aquifer leading to a deviation of the presented solution from that of Malama et al. (2008) (in which the inter-porosity flow is not considered) during the early and intermediate time when the inter-porosity flow dominates.

- In Model II, the three layers respond to the pumping well in the same manner as in the Model I and the drawdown is inversely proportional to K_{rf}/K_{ru}. However, the response is far more significant than in the Model I configuration. The vertical hydraulic conductivity of the fractures and the hydraulic conductivity of matrix blocks have no effect on the overlying unconfined aquifer and the aquitard. In contrast, the specific storage of the fractures controls the drawdown response of the all three water-bearing layers. The effect of the watertable linearization parameter, β_D, is observed in all the three layers, although it is more significant for the upper layer than for the lower layer for both models, since the underlying aquifers are less affected by the watertable drainage.
- Increasing the vertical hydraulic conductivity, K_{za}, and decreasing the specific storage, S_{sa}, and the thickness of the aquitard increases the leakage from the underlying fractured aquifer to the overlying unconfined aquifer. This influences the dimensionless drawdown in the overlying unconfined aquifer. Thus, using the presented three-layer model solution is advised for thin aquitards with a high vertical hydraulic diffusivity (K_{za}/S_{sa}).

Acknowledgment

Financial support provided by Payame Noor University and Shiraz University are acknowledged. We would like to express our sincere thanks to Dr. E. J. M. Veling for his detailed review and insightful comments and corrections. Valuable comments and suggestions from an anonymous reviewer and the Editor are also appreciated.

Appendix A

Using the dimensionless variables defined in Table 1 and taking the Laplace transformation of Eqs. (1-7) and (8-21) results in (time transformation, Laplace transform variable p):

$$\frac{1}{r_{\mathrm{D}}}\frac{\partial}{\partial r_{\mathrm{D}}}\left(r_{\mathrm{D}}\frac{\partial \bar{s}_{\mathrm{uD}}}{\partial r_{\mathrm{D}}}\right)+\alpha_{\mathrm{Dz}}^{\mathrm{u}}\frac{\partial^2 \bar{s}_{\mathrm{uD}}}{\partial z_{\mathrm{D}}^2}-p\bar{s}_{\mathrm{uD}} = 0 \tag{A1}$$

for the overlying unconfined aquifer;

$$\frac{\alpha_{\mathrm{Dr}}^{\mathrm{a}}}{r_{\mathrm{D}}}\frac{\partial}{\partial r_{\mathrm{D}}}\left(r_{\mathrm{D}}\frac{\partial \bar{s}_{\mathrm{aD}}}{\partial r_{\mathrm{D}}}\right)+\alpha_{\mathrm{Dz}}^{\mathrm{a}}\frac{\partial^2 \bar{s}_{\mathrm{aD}}}{\partial z_{\mathrm{D}}^2}-p\bar{s}_{\mathrm{aD}} = 0 \tag{A2}$$

for the aquitard and,

$$\frac{\alpha_{\mathrm{Dr}}^{\mathrm{f}}}{r_{\mathrm{D}}}\frac{\partial}{\partial r_{\mathrm{D}}}\left(r_{\mathrm{D}}\frac{\partial \bar{s}_{\mathrm{fD}}}{\partial r_{\mathrm{D}}}\right)+\alpha_{\mathrm{Dz}}^{\mathrm{f}}\frac{\partial^2 \bar{s}_{\mathrm{fD}}}{\partial z_{\mathrm{D}}^2}-(p+\gamma)\bar{s}_{\mathrm{fD}} = 0 \tag{A3}$$

for the underlying fractured aquifer. The Laplace domain far-field boundary condition is:

$$\lim_{r_{\mathrm{D}}\to\infty}\bar{s}_{\mathrm{uD}}(r_{\mathrm{D}},z_{\mathrm{D}},p) = \lim_{r_{\mathrm{D}}\to\infty}\bar{s}_{\mathrm{aD}}(r_{\mathrm{D}},z_{\mathrm{D}},p) = \lim_{r_{\mathrm{D}}\to\infty}\bar{s}_{\mathrm{fD}}(r_{\mathrm{D}},z_{\mathrm{D}},p) = 0 \tag{A4}$$

The Laplace domain boundary condition at the pumping well for the case in which it is screened in the overlying unconfined aquifer is:

$$\lim_{r_{\mathrm{D}}\to 0} r_{\mathrm{D}}\frac{\partial \bar{s}_{\mathrm{uD}}}{\partial r_{\mathrm{D}}} = \begin{cases} 0 & -d_{\mathrm{D}} < z_{\mathrm{D}} < 0 \\ -\dfrac{2}{p(l_{\mathrm{D}}-d_{\mathrm{D}})} & -l_{\mathrm{D}} < z < -d_{\mathrm{D}} \\ 0 & -1 < z < -l_{\mathrm{D}} \end{cases} \tag{A5}$$

$$\lim_{r_D\to 0} r_D\frac{\partial \bar{s}_{aD}}{\partial r_D} = 0 \tag{A6}$$

$$\lim_{r_{\mathrm{D}}\to 0} r_{\mathrm{D}}\frac{\partial \bar{s}_{\mathrm{fD}}}{\partial r_{\mathrm{D}}} = 0 \tag{A7}$$

The corresponding expressions for the case in which the well is screened in the underlying fractured aquifer are, respectively:

$$\lim_{r_D \to 0} r_D \frac{\partial \bar{s}_{fD}}{\partial r_D} = \begin{cases} 0 & -d_D < z_D < 0 \\ -\dfrac{2K_{ru}}{pK_{rf}(l_D - d_D)} & -l_D < z < -d_D \\ 0 & -1 < z < -l_D \end{cases} \tag{A8}$$

$$\lim_{r_D \to 0} r_D \frac{\partial \bar{s}_{uD}}{\partial r_D} = 0 \tag{A9}$$

$$\lim_{r_D \to 0} r_D \frac{\partial \bar{s}_{aD}}{\partial r_D} = 0 \tag{A10}$$

The Laplace domain watertable condition is:

$$\beta_D \frac{\partial^2 \bar{s}_{uD}}{\partial z_D^2}\bigg|_{z_D = 0} + \frac{\partial \bar{s}_{uD}}{\partial z_D}\bigg|_{z_D = 0} + \frac{p}{\alpha_{Dy}} \bar{s}_{uD} = 0 \tag{A11}$$

The no-flow condition is considered at the base of the fractured aquifer:

$$\frac{\partial \bar{s}_{fD}}{\partial z_D}\bigg|_{z = -b_{D3}} = 0 \tag{A12}$$

The continuity of drawdown and flux at the unconfined aquifer and the aquitard interface are, after transformation:

$$\bar{s}_{uD}(r_D, -1, p) = \bar{s}_{aD}(r_D, -1, p) \tag{A13}$$

$$K_{zu} \frac{\partial \bar{s}_{uD}}{\partial z_D}\bigg|_{z_D = -1} = K_{za} \frac{\partial \bar{s}_{aD}}{\partial z_D}\bigg|_{z_D = -1} \tag{A14}$$

Continuity of drawdown and flux at the aquitard and the fractured aquifer interface are expressed as:

$$\bar{s}_{aD}(r_D, -b_{D2}, p) = \bar{s}_{fD}(r_D, -b_{D2}, p) \tag{A15}$$

$$K_{za} \frac{\partial \bar{s}_{aD}}{\partial z_D}\bigg|_{z_D = -b_{D2}} = K_{zf} \frac{\partial \bar{s}_{fD}}{\partial z_D}\bigg|_{z_D = -b_{D2}} \tag{A16}$$

For the conceptual Model I (Fig. 1a) in which the well is screened in the overlying unconfined aquifer, Eqs. (A1-A7) and (A11-A16) are considered. As the pumping well is screened in the

overlying unconfined aquifer (Eqs. A5-A7), the dimensionless drawdown in Eq. (A1) should be decomposed as $\bar{s}_{\mathrm{uD}} = u_{\mathrm{D}} + v_{\mathrm{D}}$ (Neuman, 1974; Malama et al., 2008). For the first term, u_{D}, the governing equation is:

$$\frac{1}{r_{\mathrm{D}}}\frac{\partial}{\partial r_{\mathrm{D}}}\left(r_{\mathrm{D}}\frac{\partial u_{\mathrm{D}}}{\partial r_{\mathrm{D}}}\right) + \alpha_{\mathrm{Dz}}^{\mathrm{u}}\frac{\partial^2 u_{\mathrm{D}}}{\partial z_{\mathrm{D}}^2} - p u_{\mathrm{D}} = 0 \tag{A17}$$

subject to the following boundary conditions:

$$\lim_{r_{\mathrm{D}}\to\infty} u_{\mathrm{D}}(r_{\mathrm{D}}, z_{\mathrm{D}}, \mathrm{p}) = 0 \tag{A18}$$

$$\lim_{r_{\mathrm{D}}\to 0} r_{\mathrm{D}}\frac{\partial u_{\mathrm{D}}}{\partial r_{\mathrm{D}}} = \begin{cases} 0 & -d_{\mathrm{D}} < z_{\mathrm{D}} < 0 \\ -\dfrac{2}{p(l_{\mathrm{D}} - d_{\mathrm{D}})} & -l_{\mathrm{D}} < z < -d_{\mathrm{D}} \\ 0 & -1 < z < -l_{\mathrm{D}} \end{cases} \tag{A19}$$

$$\left.\frac{\partial u_{\mathrm{D}}}{\partial z_{\mathrm{D}}}\right|_{z_{\mathrm{D}}=0} = \left.\frac{\partial u_{\mathrm{D}}}{\partial z_{\mathrm{D}}}\right|_{z_{\mathrm{D}}=-1} = 0 \tag{A20}$$

For the second term, v_{D}, the following governing equation is considered:

$$\frac{1}{r_{\mathrm{D}}}\frac{\partial}{\partial r_{\mathrm{D}}}\left(r_{\mathrm{D}}\frac{\partial v_{\mathrm{D}}}{\partial r_{\mathrm{D}}}\right) + \alpha_{\mathrm{Dz}}^{\mathrm{u}}\frac{\partial^2 v_{\mathrm{D}}}{\partial z_{\mathrm{D}}^2} - p v_{\mathrm{D}} = 0 \tag{A21}$$

subject to the following boundary conditions:

$$\lim_{r_{\mathrm{D}}\to 0} r_{\mathrm{D}}\frac{\partial v_{\mathrm{D}}}{\partial r_{\mathrm{D}}} = 0 \tag{A22}$$

$$\beta_{\mathrm{D}}\left.\frac{\partial^2 v_{\mathrm{D}}}{\partial z_{\mathrm{D}}^2}\right|_{z_{\mathrm{D}}=0} + \beta_{\mathrm{D}}\left.\frac{\partial^2 u_{\mathrm{D}}}{\partial z_{\mathrm{D}}^2}\right|_{z_{\mathrm{D}}=0} + \left.\frac{\partial v_{\mathrm{D}}}{\partial z_{\mathrm{D}}}\right|_{z_{\mathrm{D}}=0} + \left.\frac{p}{\alpha_{\mathrm{Dy}}}(u_{\mathrm{D}} + v_{\mathrm{D}})\right|_{z_{\mathrm{D}}=0} = 0 \tag{A23}$$

Applying the Hankel transform to Eqs. (A17), (A20), (A21) and (A23) with respect to boundary conditions of Eqs. (A18), (A19) and (A22) results in:

$$\frac{\partial^2 \hat{u}_\mathrm{D}}{\partial z_\mathrm{D}^2} - \eta_\mathrm{u}^2 \hat{u}_\mathrm{D} = \frac{1}{\alpha_\mathrm{Dz}^\mathrm{u}} \lim_{r_\mathrm{D}\to 0} r_\mathrm{D} \frac{\partial u_\mathrm{D}}{\partial r_\mathrm{D}} \tag{A24}$$

subject to the following boundary conditions:

$$\lim_{r_\mathrm{D}\to 0} r_\mathrm{D} \frac{\partial u_\mathrm{D}}{\partial r_\mathrm{D}} = \begin{cases} 0 & -d_\mathrm{D} < z_\mathrm{D} < 0 \\ -\dfrac{2}{p(l_\mathrm{D} - d_\mathrm{D})} & -l_\mathrm{D} < z < -d_\mathrm{D} \\ 0 & -1 < z < -l_\mathrm{D} \end{cases} \tag{A25}$$

$$\left.\frac{\partial \hat{u}_\mathrm{D}}{\partial z_\mathrm{D}}\right|_{z_\mathrm{D}=0} = \left.\frac{\partial \hat{u}_\mathrm{D}}{\partial z_\mathrm{D}}\right|_{z_\mathrm{D}=-1} = 0 \tag{A26}$$

For $\hat{v}_\mathrm{D}$, the governing equation is:

$$\frac{\partial^2 \hat{v}_\mathrm{D}}{\partial z_\mathrm{D}^2} - \eta_\mathrm{u}^2 \hat{v}_\mathrm{D} = 0 \tag{A27}$$

which is solved subject to the following boundary condition:

$$\beta_\mathrm{D} \left.\frac{\partial^2 \hat{v}_\mathrm{D}}{\partial z_\mathrm{D}^2}\right|_{z_\mathrm{D}=0} + \beta_\mathrm{D} \left.\frac{\partial^2 \hat{u}_\mathrm{D}}{\partial z_\mathrm{D}^2}\right|_{z_\mathrm{D}=0} + \left.\frac{\partial \hat{v}_\mathrm{D}}{\partial z_\mathrm{D}}\right|_{z_\mathrm{D}=0} + \left.\frac{p}{\alpha_\mathrm{Dy}}(\hat{u}_\mathrm{D} + \hat{v}_\mathrm{D})\right|_{z_\mathrm{D}=0} = 0 \tag{A28}$$

Equation (A24) is solved subject to boundary conditions given by Eqs. (A25) and (A26) as in Malama et al. (2008, Eqs. A9-A11 and 22) as:

$$\hat{u}_\mathrm{D}(a, z_\mathrm{D}, p) = \frac{2[\cosh(\eta_\mathrm{u}\zeta_\mathrm{D}) + \delta \hat{u}_\mathrm{D}(\eta_\mathrm{u}, z_\mathrm{D})]}{p\eta_\mathrm{u}^2 \alpha_\mathrm{Dz}^\mathrm{u}(l_\mathrm{D} - d_\mathrm{D})} \tag{A29}$$

where

$$\zeta_\mathrm{D} = \begin{cases} d_\mathrm{D} + z_\mathrm{D} & \forall z_\mathrm{D} \in (-d_\mathrm{D}, 0] \\ 0 & \forall z_\mathrm{D} \in [-l_\mathrm{D}, -d_\mathrm{D}] \\ l_\mathrm{D} + z_\mathrm{D} & \forall z_\mathrm{D} \in [-1, -l_\mathrm{D}) \end{cases} \tag{A30}$$

and

$$\delta\hat{u}_{\mathrm{D}}(\eta_{\mathrm{u}}, z_{\mathrm{D}}) = \frac{\sinh(\eta_{\mathrm{u}} d_{\mathrm{D}})\cosh[\eta_{\mathrm{u}}(1+z_{\mathrm{D}})]+\sinh[\eta_{\mathrm{u}}(1-l_{\mathrm{D}})]\cosh(\eta_{\mathrm{u}} z_{\mathrm{D}})}{\sinh(\eta_{\mathrm{u}})} \tag{A31}$$

For the aquitard, the Laplace-Hankel space governing equation is:

$$\frac{\partial^2 \hat{\bar{s}}_{\mathrm{aD}}}{\partial z_{\mathrm{D}}^2} - \eta_{\mathrm{a}}^2 \hat{\bar{s}}_{\mathrm{aD}} = 0 \tag{A32}$$

The boundary conditions at the unconfined aquifer and the aquitard are:

$$\hat{v}_{\mathrm{D}}(a, -1, p) + \hat{u}_{\mathrm{D}}(a, -1, p) = \hat{\bar{s}}_{\mathrm{aD}}(a, -1, p) \tag{A33}$$

$$\left.\frac{\partial \hat{v}_{\mathrm{D}}}{\partial z_{\mathrm{D}}}\right|_{z_{\mathrm{D}}=-1} = \gamma_1 \left.\frac{\partial \hat{\bar{s}}_{\mathrm{aD}}}{\partial z_{\mathrm{D}}}\right|_{z_{\mathrm{D}}=-1} \tag{A34}$$

where

$$\gamma_1 = \frac{\eta_{\mathrm{a}}}{\eta_{\mathrm{u}}} \frac{K_{\mathrm{za}}}{K_{\mathrm{zu}}} \tag{A35}$$

For the underlying fractured aquifer the Laplace-Hankel space governing equation is:

$$\frac{\partial^2 \hat{\bar{s}}_{\mathrm{fD}}}{\partial z_{\mathrm{D}}^2} - \eta_{\mathrm{f}}^2 \hat{\bar{s}}_{\mathrm{fD}} = 0 \tag{A36}$$

The boundary conditions at the aquitard and the fractured aquifer interface are:

$$\hat{\bar{s}}_{\mathrm{aD}}(a, -b_{\mathrm{D2}}, p) = \hat{\bar{s}}_{\mathrm{fD}}(a, -b_{\mathrm{D2}}, p) \tag{A37}$$

$$\left.\frac{\partial \hat{\bar{s}}_{\mathrm{aD}}}{\partial z_{\mathrm{D}}}\right|_{z_{\mathrm{D}}=-b_{\mathrm{D2}}} = \gamma_2 \left.\frac{\partial \hat{\bar{s}}_{\mathrm{fD}}}{\partial z_{\mathrm{D}}}\right|_{z_{\mathrm{D}}=-b_{\mathrm{D2}}} \tag{A38}$$

where

$$\gamma_2 = \frac{\eta_{\mathrm{f}}}{\eta_{\mathrm{a}}} \frac{K_{\mathrm{zf}}}{K_{\mathrm{za}}} \tag{A39}$$

Equations (A27), (A32) and (A36) are solved with respect to boundary conditions given in Eqs. (A28), (A33), (A34), (A37) and (A38) as:

$$\hat{v}_{\mathrm{D}} = c_1 \exp(\eta_{\mathrm{u}} z_{\mathrm{D}}) + c_2 \exp(-\eta_{\mathrm{u}} z_{\mathrm{D}}) \tag{A40}$$

$$\hat{\bar{s}}_{\mathrm{aD}} = c_3 \exp(\eta_{\mathrm{a}} z_{\mathrm{D}}) + c_4 \exp(-\eta_{\mathrm{a}} z_{\mathrm{D}}) \tag{A41}$$

$$\hat{\bar{s}}_{\mathrm{fD}} = c_5 \exp(\eta_{\mathrm{f}} z_{\mathrm{D}}) + c_6 \exp(-\eta_{\mathrm{f}} z_{\mathrm{D}}) \tag{A42}$$

The constants in the above equations are obtained using Maple. It should be noted that the constants c_3 and c_4 are obtained at the first step and simplified, then the constants c_1, c_2, $c_5$and c_6 are obtained at the second step as (the reader may refer to supplementary materials for the Maple script):

$$c_1 = \frac{1}{2}\frac{c_3\gamma_1 \exp(-\eta_{\mathrm{a}}) - c_4\gamma_1 \exp(\eta_{\mathrm{a}}) + c_3 \exp(-\eta_{\mathrm{a}}) + c_4 \exp(\eta_{\mathrm{a}}) - \hat{u}_{\mathrm{D}}(-1)}{\exp(-\eta_{\mathrm{u}})} \tag{A43}$$

$$c_2 = -\frac{1}{2}\frac{c_3\gamma_1 \exp(-\eta_{\mathrm{a}}) - c_4\gamma_1 \exp(\eta_{\mathrm{a}}) - c_3 \exp(-\eta_{\mathrm{a}}) - c_4 \exp(\eta_{\mathrm{a}}) + \hat{u}_{\mathrm{D}}(-1)}{\exp(\eta_{\mathrm{u}})} \tag{A44}$$

$$c_5 = \frac{1}{2}\frac{c_3\gamma_2 \exp(-\eta_{\mathrm{a}} b_{\mathrm{D2}}) + c_4\gamma_2 \exp(\eta_{\mathrm{a}} b_{\mathrm{D2}}) + c_3 \exp(-\eta_{\mathrm{a}} b_{\mathrm{D2}}) - c_4 \exp(\eta_{\mathrm{a}} b_{\mathrm{D2}})}{\gamma_2 \exp(-\eta_{\mathrm{f}} b_{\mathrm{D2}})} \tag{A45}$$

$$c_6 = \frac{1}{2}\frac{c_3\gamma_2 \exp(-\eta_{\mathrm{a}} b_{\mathrm{D2}}) + c_4\gamma_2 \exp(\eta_{\mathrm{a}} b_{\mathrm{D2}}) - c_3 \exp(-\eta_{\mathrm{a}} b_{\mathrm{D2}}) + c_4 \exp(\eta_{\mathrm{a}} b_{\mathrm{D2}})}{\gamma_2 \exp(\eta_{\mathrm{f}} b_{\mathrm{D2}})} \tag{A46}$$

$$c_3 = \frac{exp(\eta_a b_{D2})(\psi_1 + \psi_2 + \psi_3)}{\chi} \tag{A47}$$

$$c_4 = \frac{\exp(-\eta_{\mathrm{a}} b_{\mathrm{D2}})(\psi_1 - \psi_2 + \psi_4)}{\chi} \tag{A48}$$

where

$$\begin{aligned}\chi = {} & 2\{\sinh(\theta_1 + \eta_{\mathrm{a}}) + \sinh(\theta_2 + \eta_{\mathrm{a}})\}\{\sigma\gamma_1\gamma_2 \exp(-\eta_{\mathrm{u}}) \\ & + \vartheta\gamma_1\gamma_2 \exp(\eta_{\mathrm{u}})\} + \\ & 2\{-\cosh(\theta_1 + \eta_{\mathrm{a}}) + \cosh(\theta_2 + \eta_{\mathrm{a}})\}\{\sigma\gamma_1 \exp(-\eta_{\mathrm{u}}) + \vartheta\gamma_1 \exp(\eta_{\mathrm{u}})\} + \\ & 2\{-\cosh(\theta_1 + \eta_{\mathrm{a}}) + \cosh(\theta_2 + \eta_{\mathrm{a}})\}\{\sigma\gamma_2 \exp(-\eta_{\mathrm{u}}) + \vartheta\gamma_2 \exp(\eta_{\mathrm{u}})\} + \\ & 2\{\cosh(\theta_1 + \eta_{\mathrm{a}}) + \cosh(\theta_2 + \eta_{\mathrm{a}})\}\{\sigma \exp(-\eta_{\mathrm{u}}) + \vartheta \exp(\eta_{\mathrm{u}})\}\end{aligned} \tag{A49}$$

$$\theta_1 = \eta_{\mathrm{f}} b_{\mathrm{D3}} - \eta_{\mathrm{a}} b_{\mathrm{D2}} - \eta_{\mathrm{f}} b_{\mathrm{D2}} \tag{A50}$$

$$\theta_2 = -\eta_{\mathrm{f}} b_{\mathrm{D3}} - \eta_{\mathrm{a}} b_{\mathrm{D2}} + \eta_{\mathrm{f}} b_{\mathrm{D2}} \tag{A51}$$

$$\psi_1 = 2\sinh(\eta_{\mathrm{f}} b_{\mathrm{D3}} - \eta_{\mathrm{f}} b_{\mathrm{D2}})\{\vartheta\gamma_2\hat{u}_{\mathrm{D}}(-1)\exp(-\eta_{\mathrm{u}}) + \sigma\gamma_2\hat{u}_{\mathrm{D}}(-1)\exp(\eta_{\mathrm{u}})\} \tag{A52}$$

$$\psi_2 = 2\cosh(-\eta_{\mathrm{f}} b_{\mathrm{D3}} + \eta_{\mathrm{f}} b_{\mathrm{D2}})\{\vartheta\hat{u}_{\mathrm{D}}(-1)\exp(\eta_{\mathrm{u}}) - \sigma\hat{u}_{\mathrm{D}}(-1)\exp(-\eta_{\mathrm{u}})\} \tag{A53}$$

$$\psi_3 = 4(1+\beta_{\mathrm{D}}\eta_u\xi)\hat{u}_{\mathrm{D}}(0)\{\gamma_2\sinh(-\eta_{\mathrm{f}} b_{\mathrm{D3}} + \eta_{\mathrm{f}} b_{\mathrm{D2}}) - \cosh(-\eta_{\mathrm{f}} b_{\mathrm{D3}} + \eta_{\mathrm{f}} b_{\mathrm{D2}})\} \tag{A54}$$

$$\psi_4 = 4(1+\beta_{\mathrm{D}}\eta_u\xi)\hat{u}_{\mathrm{D}}(0)\{\gamma_2\sinh(-\eta_{\mathrm{f}} b_{\mathrm{D3}} + \eta_{\mathrm{f}} b_{\mathrm{D2}}) + \cosh(-\eta_{\mathrm{f}} b_{\mathrm{D3}} + \eta_{\mathrm{f}} b_{\mathrm{D2}})\} \tag{A55}$$

where

$$\vartheta = \xi + 1 + \beta_{\mathrm{D}}\eta_{\mathrm{u}}\xi \tag{A56}$$

$$\sigma = \xi - 1 - \beta_{\mathrm{D}}\eta_{\mathrm{u}}\xi \tag{A57}$$

Equations (A40-A42) are used to obtain Eqs. (22-24) after carrying out the inverse Hankel transform.

Appendix B

Equations (A1-A4) and (A8-A15) are solved for conceptual Model II (Fig. 1b) in which the pumping well is screened in the underlying fractured aquifer. Following the same procedure as in Appendix A, the Laplace-Hankel domain governing equations and boundary conditions are given below.

The governing equation for the overlying unconfined aquifer is:

$$\frac{\partial^2 \hat{\bar{s}}_{\mathrm{uD}}}{\partial z_{\mathrm{D}}^2} - \eta_{\mathrm{u}}^2 \hat{\bar{s}}_{\mathrm{uD}} = 0 \tag{B1}$$

The watertable boundary condition is:

$$\beta_{\mathrm{D}} \frac{\partial^2 \hat{\bar{s}}_{\mathrm{uD}}}{\partial z_{\mathrm{D}}^2}\bigg|_{z_{\mathrm{D}}=0} + \frac{\partial \hat{\bar{s}}_{\mathrm{uD}}}{\partial z_{\mathrm{D}}}\bigg|_{z_{\mathrm{D}}=0} + \frac{p}{\alpha_{\mathrm{Dy}}} \hat{\bar{s}}_{\mathrm{uD}}\bigg|_{z_{\mathrm{D}}=0} = 0 \tag{B2}$$

The boundary conditions at the unconfined aquifer-aquitard interface are:

$$\hat{\bar{s}}_{\mathrm{uD}}(a,-1,p) = \hat{\bar{s}}_{\mathrm{aD}}(a,-1,p) \tag{B3}$$

$$\frac{\partial \hat{\bar{s}}_{\mathrm{uD}}}{\partial z_{\mathrm{D}}}\bigg|_{z_{\mathrm{D}}=-1} = \gamma_1 \frac{\partial \hat{\bar{s}}_{\mathrm{aD}}}{\partial z_{\mathrm{D}}}\bigg|_{z_{\mathrm{D}}=-1} \tag{B4}$$

The governing equation for the aquitard is:

$$\frac{\partial^2 \hat{\bar{s}}_{\mathrm{aD}}}{\partial z_{\mathrm{D}}^2} - \eta_{\mathrm{a}}^2 \hat{\bar{s}}_{\mathrm{aD}} = 0 \tag{B5}$$

The boundary conditions at the aquitard-fractured aquifer interface are:

$$\hat{\bar{s}}_{\mathrm{aD}}(a,-b_{\mathrm{D2}},p) = \hat{\bar{s}}_{\mathrm{fD}}(a,-b_{\mathrm{D2}},p) \tag{B6}$$

$$\frac{\partial \hat{\bar{s}}_{\mathrm{aD}}}{\partial z_{\mathrm{D}}}\bigg|_{z_{\mathrm{D}}=-b_{\mathrm{D2}}} = \gamma_2 \frac{\partial \hat{\bar{s}}_{\mathrm{fD}}}{\partial z_{\mathrm{D}}}\bigg|_{z_{\mathrm{D}}=-b_{\mathrm{D2}}} \tag{B7}$$

The governing equation for the underlying fractured aquifer is:

$$\frac{\partial^2 \hat{\bar{s}}_{\mathrm{fD}}}{\partial z_{\mathrm{D}}^2} - \eta_{\mathrm{f}}^2 \hat{\bar{s}}_{\mathrm{fD}} = 0 \tag{B8}$$

As the pumping well is screened in the underlying fractured aquifer (Eqs. A8-A10), Eqs. (B6-B8) can be decomposed as $\hat{\bar{s}}_{\mathrm{fD}} = \hat{u}_{\mathrm{D}} + \hat{v}_{\mathrm{D}}$, which results in the following governing equations and boundary conditions:

$$\frac{\partial^2 \hat{u}_{\mathrm{D}}}{\partial z_{\mathrm{D}}^2} - \eta_{\mathrm{f}}^2 \hat{u}_{\mathrm{D}} = \frac{1}{\alpha_{\mathrm{Dz}}^{\mathrm{f}}} \lim_{r_{\mathrm{D}}\to 0} r_{\mathrm{D}} \frac{\partial u_{\mathrm{D}}}{\partial r_{\mathrm{D}}} \tag{B9}$$

where

$$\lim_{r_\mathrm{D}\to 0}\left(r_\mathrm{D}\frac{\partial u_\mathrm{D}}{\partial r_\mathrm{D}}\right)\begin{cases} 0 & -d_\mathrm{D} < z_\mathrm{D} < -b_{\mathrm{D}2} \\ -\frac{2}{p(l_\mathrm{D}-d_\mathrm{D})} & -l_\mathrm{D} < z < -d_\mathrm{D} \\ 0 & -b_{\mathrm{D}3} < z < -l_\mathrm{D} \end{cases} \tag{B10}$$

subject to the following boundary condition:

$$\left.\frac{\partial \hat{u}_\mathrm{D}}{\partial z_\mathrm{D}}\right|_{z_\mathrm{D}=-b_{\mathrm{D}2}} = \left.\frac{\partial \hat{u}_\mathrm{D}}{\partial z_\mathrm{D}}\right|_{z_\mathrm{D}=-b_{\mathrm{D}3}} = 0 \tag{B11}$$

For $\hat{v}_\mathrm{D}$, the model to be solved is:

$$\frac{\partial^2 \hat{v}_\mathrm{D}}{\partial z_\mathrm{D}^2} - \eta_\mathrm{u}^2 \hat{v}_\mathrm{D} = 0 \tag{B12}$$

subject to the following boundary conditions:

$$\hat{u}_\mathrm{D}(a,-b_{\mathrm{D}2},p) + \hat{v}_\mathrm{D}(a,-b_{\mathrm{D}2},p) = \hat{\bar{s}}_\mathrm{aD}(a,-b_{\mathrm{D}2},p) \tag{B13}$$

$$\left.\frac{\partial \hat{v}_\mathrm{D}}{\partial z_\mathrm{D}}\right|_{z_\mathrm{D}=-b_{\mathrm{D}2}} = \gamma_2 \left.\frac{\partial \hat{\bar{s}}_\mathrm{aD}}{\partial z_\mathrm{D}}\right|_{z_\mathrm{D}=-b_{\mathrm{D}2}} \tag{B14}$$

$$\left.\frac{\partial \hat{v}_\mathrm{D}}{\partial z_\mathrm{D}}\right|_{z_\mathrm{D}=-b_{\mathrm{D}3}} = 0 \tag{B15}$$

The same procedure as in Appendix A is followed to solve Eqs. (B1), (B5), (B9) and (B12) subject to the boundary conditions Eqs. (B2-B4), (B11) and (B13-B15), giving:

$$\hat{\bar{s}}_\mathrm{uD} = c_1\exp(\eta_\mathrm{u} z_\mathrm{D}) + c_2\exp(-\eta_\mathrm{u} z_\mathrm{D}) \tag{B16}$$

$$\hat{\bar{s}}_\mathrm{aD} = c_3\exp(\eta_\mathrm{a} z_\mathrm{D})e^{\eta_\mathrm{a} z_\mathrm{D}} + c_4\exp(-\eta_\mathrm{a} z_\mathrm{D}) \tag{B17}$$

$$\hat{\bar{s}}_\mathrm{fD} = \hat{u}_\mathrm{D} + c_5\exp(\eta_\mathrm{f} z_\mathrm{D}) + c_6\exp(-\eta_\mathrm{f} z_\mathrm{D}) \tag{B18}$$

where the solution for cases of $\hat{u}_\mathrm{D}$ in different parts of the aquifer is obtained following the same procedure as Malama et al. (2008):

$$\hat{u}_\mathrm{D} = A_1\exp(\eta_\mathrm{u} z_\mathrm{D}) + B_1\exp(-\eta_\mathrm{u} z_\mathrm{D}),\ -d_\mathrm{D} < z_\mathrm{D} < -b_{\mathrm{D}2} \tag{B19}$$

$$\hat{u}_{\mathrm{D}} = A_2\exp(\eta_{\mathrm{u}} z_{\mathrm{D}}) + B_2\exp(-\eta_{\mathrm{u}} z_{\mathrm{D}}),\ -b_{\mathrm{D3}} < z_{\mathrm{D}} < -l_{\mathrm{D}} \tag{B20}$$

$$\hat{u}_{\mathrm{D}} = A_3\exp(\eta_{\mathrm{u}} z_{\mathrm{D}}) + B_3\exp(-\eta_{\mathrm{u}} z_{\mathrm{D}}) + \frac{2}{p\eta_{\mathrm{f}}^2\alpha_{\mathrm{Dz}}^{\mathrm{f}}(l_{\mathrm{D}} - d_{\mathrm{D}})},\ -l_{\mathrm{D}} < z_{\mathrm{D}} < -d_{\mathrm{D}} \tag{B21}$$

$$A_1 = \frac{\exp(\eta_{\mathrm{f}} d_{\mathrm{D}}) - w_{\mathrm{D},1}}{p\eta_{\mathrm{f}}^2\alpha_{\mathrm{Dz}}^{\mathrm{f}}(l_{\mathrm{D}} - d_{\mathrm{D}})} \tag{B22}$$

$$B_1 = \frac{\exp(-\eta_{\mathrm{f}} d_{\mathrm{D}}) - w_{\mathrm{D},2}}{p\eta_{\mathrm{f}}^2\alpha_{\mathrm{Dz}}^{\mathrm{f}}(l_{\mathrm{D}} - d_{\mathrm{D}})} \tag{B23}$$

$$A_2 = \frac{\exp(\eta_{\mathrm{f}} l_{\mathrm{D}}) - w_{\mathrm{D},1}}{p\eta_{\mathrm{f}}^2\alpha_{\mathrm{Dz}}^{\mathrm{f}}(l_{\mathrm{D}} - d_{\mathrm{D}})} \tag{B24}$$

$$B_2 = \frac{\exp(-\eta_{\mathrm{f}} l_{\mathrm{D}}) - w_{\mathrm{D},2}}{p\eta_{\mathrm{f}}^2\alpha_{\mathrm{Dz}}^{\mathrm{f}}(l_{\mathrm{D}} - d_{\mathrm{D}})} \tag{B25}$$

$$A_3 = \frac{-w_{\mathrm{D},1}}{p\eta_{\mathrm{f}}^2\alpha_{\mathrm{Dz}}^{\mathrm{f}}(l_{\mathrm{D}} - d_{\mathrm{D}})} \tag{B26}$$

$$B_3 = \frac{-w_{\mathrm{D},2}}{p\eta_{\mathrm{f}}^2\alpha_{\mathrm{Dz}}^{\mathrm{f}}(l_{\mathrm{D}} - d_{\mathrm{D}})} \tag{B27}$$

$$w_{\mathrm{D},1} = \frac{\exp(\eta_{\mathrm{f}} b_{\mathrm{D3}})\sinh(-\eta_{\mathrm{f}} b_{\mathrm{D2}} + \eta_{\mathrm{f}} d_{\mathrm{D}}) + \exp(\eta_{\mathrm{f}} b_{\mathrm{D3}})\sinh(\eta_{\mathrm{f}} b_{\mathrm{D3}} - \eta_{\mathrm{f}} l_{\mathrm{D}})}{\sinh(-\eta_{\mathrm{f}} b_{\mathrm{D2}} + \eta_{\mathrm{f}} b_{\mathrm{D3}})} \tag{B28}$$

$$w_{\mathrm{D},2} = \frac{\exp(-\eta_{\mathrm{f}} b_{\mathrm{D3}})\sinh(-\eta_{\mathrm{f}} b_{\mathrm{D2}} + \eta_{\mathrm{f}} d_{\mathrm{D}}) + \exp(-\eta_{\mathrm{f}} b_{\mathrm{D3}})\sinh(\eta_{\mathrm{f}} b_{\mathrm{D3}} - \eta_{\mathrm{f}} l_{\mathrm{D}})}{\sinh(-\eta_{\mathrm{f}} b_{\mathrm{D2}} + \eta_{\mathrm{f}} b_{\mathrm{D3}})} \tag{B29}$$

To obtain c_1-c_6 the same procedure as in Appendix A are followed (Please see supplementary materials for the Maple script)

$$c_1 = \frac{c_3\gamma_1\exp(-\eta_{\mathrm{a}}) - c_4\gamma_1\exp(\eta_{\mathrm{a}}) + c_3\exp(-\eta_{\mathrm{a}}) + c_4\exp(\eta_{\mathrm{a}})}{2\exp(-\eta_{\mathrm{u}})} \tag{B30}$$

$$c_2 = -\frac{c_3\gamma_1\exp(-\eta_{\mathrm{a}}) - c_4\gamma_1\exp(\eta_{\mathrm{a}}) - c_3\exp(-\eta_{\mathrm{a}}) - c_4\exp(\eta_{\mathrm{a}})}{2\exp(\eta_{\mathrm{u}})} \tag{B31}$$

$$c_5 = \frac{c_3\gamma_2\exp(-\eta_\mathrm{a}b_{\mathrm{D}2}) + c_4\gamma_2\exp(\eta_\mathrm{a}b_{\mathrm{D}2}) + c_3\exp(-\eta_\mathrm{a}b_{\mathrm{D}2}) - c_4\exp(\eta_\mathrm{a}b_{\mathrm{D}2}) - \gamma_2\hat{u}_\mathrm{D}(-b_{\mathrm{D}2})}{2\gamma_2\exp(-\eta_\mathrm{f}b_{\mathrm{D}3})} \tag{B32}$$

$$c_6 = \frac{c_3\gamma_2\exp(-\eta_\mathrm{a}b_{\mathrm{D}2}) + c_4\gamma_2\exp(\eta_\mathrm{a}b_{\mathrm{D}2}) - c_3\exp(-\eta_\mathrm{a}b_{\mathrm{D}2}) + c_4\exp(\eta_\mathrm{a}b_{\mathrm{D}2}) - \gamma_2\hat{u}_\mathrm{D}(-b_{\mathrm{D}2})}{2\gamma_2\exp(\eta_\mathrm{f}b_{\mathrm{D}3})} \tag{B33}$$

$$c_3 = \frac{2\{\sigma\exp(-\eta_\mathrm{u})(\gamma_1+1) + \vartheta\exp(\eta_\mathrm{u})(\gamma_1-1)\}\sinh(\eta_\mathrm{f}b_{\mathrm{D}3} - \eta_\mathrm{f}b_{\mathrm{D}2})\gamma_2\exp(\eta_\mathrm{a})\hat{u}_\mathrm{D}(-b_{\mathrm{D}2})}{\chi} \tag{B34}$$

$$c_4 = \frac{2\{\sigma\exp(-\eta_\mathrm{u})(\gamma_1-1) + \vartheta\exp(\eta_\mathrm{u})(\gamma_1+1)\}\sinh(\eta_\mathrm{f}b_{\mathrm{D}3} - \eta_\mathrm{f}b_{\mathrm{D}2})\gamma_2\exp(-\eta_\mathrm{a})\hat{u}_\mathrm{D}(-b_{\mathrm{D}2})}{\chi} \tag{B35}$$

with

$$\begin{aligned}\chi = {} & 2\{\sinh(\theta_1+\eta_\mathrm{a}) + \sinh(\theta_2+\eta_\mathrm{a})\}\{\sigma\gamma_1\gamma_2\exp(-\eta_\mathrm{u}) \\ & + \vartheta\gamma_1\gamma_2\exp(\eta_\mathrm{u})\} + \\ & 2\{-\sinh(\theta_1+\eta_\mathrm{a}) + \sinh(\theta_2+\eta_\mathrm{a})\}\{\sigma\gamma_1\exp(-\eta_\mathrm{u}) + \vartheta\gamma_1\exp(\eta_\mathrm{u})\} + \\ & 2\{\cosh(\theta_1+\eta_\mathrm{a}) + \cosh(\theta_2+\eta_\mathrm{a})\}\{\sigma\gamma_2\exp(-\eta_\mathrm{u}) + \vartheta\gamma_2\exp(\eta_\mathrm{u})\} + \\ & 2\{\cosh(\theta_1+\eta_\mathrm{a}) - \cosh(\theta_2+\eta_\mathrm{a})\}\{\sigma\exp(-\eta_\mathrm{u}) + \vartheta\exp(-\eta_\mathrm{u})\}\end{aligned} \tag{B36}$$

$$\theta_1 = \eta_\mathrm{f}b_{\mathrm{D}3} - \eta_\mathrm{a}b_{\mathrm{D}2} - \eta_\mathrm{f}b_{\mathrm{D}2} \tag{B37}$$

$$\theta_2 = -\eta_\mathrm{f}b_{\mathrm{D}3} - \eta_\mathrm{a}b_{\mathrm{D}2} + \eta_\mathrm{f}b_{\mathrm{D}2} \tag{B38}$$

$$\vartheta = \xi + 1 + \beta_\mathrm{D}\eta_\mathrm{u}\xi \tag{B39}$$

$$\sigma = \xi - 1 - \beta_\mathrm{D}\eta_\mathrm{u}\xi \tag{B40}$$

Equations (B16-B21) are used to obtain Eqs. (25-27) after taking the inverse Hankel transform.

References

Al-Shaibani, A.M., 2008. Hydrogeology and hydrochemistry of a shallow alluvial aquifer, western Saudi Arabia. Hydrogeol. J. 16, 155-165. DOI: 10.1007/s10040-007-0220-y.

Barenblatt, G., Zheltov, Iu.P., Kochina, I.N., 1960. Basic concepts in the theory of seepage of homogeneous liquids in fissured rocks [strata]. J. Appl. Math. Mech. 24, 1286-1303. DOI: 10.1016/0021-8928(60)90107-6.

Boulton, N., Streltsova, T., 1977. Unsteady flow to a pumped well in a fissured water-bearing formation. J. Hydrol. 35, 257-270. DOI: 10.1016/0022-1694(77)90005-1.

Bourdet, D., Gringarten, A.C., 1980. Determination of fissure volume and block size in fractured reservoirs by type-curve analysis. In: SPE Annual Technical Conference and Exhibition, 21-24 September, Dallas, Texas, Document ID SPE-9293-MS. Society of Petroleum Engineers. DOI: 10.2118/9293-MS.

Dagan, G., 1967. Linearized solutions of free-surface groundwater flow with uniform recharge. Journal of Geophysical Research, 72(4): 1183-1193.

De Hoog, F.R., Knight, J., Stokes, A., 1982. An improved method for numerical inversion of Laplace transforms. SIAM J. Sci. Stat. Comput. 3, 357-366. DOI: 10.1137/0903022.

Deruyck, B.G., Bourdet, D.P., DaPrat, G., Ramey Jr., H.J., 1982. Interpretation of interference tests in reservoirs with double porosity behavior: Theory and field examples. In: SPE Annual Technical Conference and Exhibition, 26-29 September, New Orleans, Louisiana, Document ID SPE-11025-MS. Society of Petroleum Engineers. DOI: 10.2118/11025-MS.

Doherty, J., Brebber, L., Whyte, P., 1994. PEST: Model-independent parameter estimation. Watermark Computing, Corinda, Australia, 122.

Duguid, J.O., Lee, P., 1977. Flow in fractured porous media. Water Resour. Res. 13, 558-566. DOI: 10.1029/WR013i003p00558.

Gringarten, A.C., Burgess, T.M., Viturat, D., Pelissier, J., Aubry, M., 1981. Evaluating fissured formation geometry from well test data: A field example. In: SPE Annual Technical Conference and Exhibition, 4-7 October, San Antonio, Texas, Document ID SPE-10182-MS. Society of Petroleum Engineers. DOI: 10.2118/10182-MS.

Hantush, M.S., 1960. Modification of the theory of leaky aquifers. J. Geophys. Res. 65, 3713-3725. DOI: 10.1029/JZ065i011p03713.

Hantush, M.S., 1967. Growth and decay of groundwater mounds in response to uniform percolation. Water Resour. Res. 3, 227-234. DOI: 10.1029/WR003i001p00227.

Hantush, M.S., Jacob, C.E., 1955. Non-steady radial flow in an infinite leaky aquifer. Eos, Trans. Amer. Geophys. Union 36, 95-100. DOI: 10.1029/TR036i001p00095.

Huang, Y.-C., Yeh, H.-D., 2007. The use of sensitivity analysis in on-line aquifer parameter estimation. J. Hydrol. 335, 406-418. DOI:10.1016/j.jhydrol.2006.12.007.

Hunt, B., 2005. Flow to vertical and nonvertical wells in leaky aquifers. J. Hydrol. Eng. 10, 477-484. DOI: 10.1061/(ASCE)1084-0699(2005)10:6(477).

Issar, A. 1969. The groundwater provinces of Iran. Hydrol. Sci. J. 14, 87-99. DOI: 10.1080/02626666909493704.

Kazemi, H., Merrill Jr., L.S., Porterfield, K.L., Zeman, P.R., 1976. Numerical simulation of water-oil flow in naturally fractured reservoirs. Soc. Petrol. Eng. J. 16, 317-326. DOI: 10.2118/5719-PA.

Liang, X., Zhan, H., You-Kuan, Z., Liu, J., 2017a. On the coupled unsaturated-saturated flow process induced by vertical, horizontal, and slant wells in unconfined aquifers. Hydrology and Earth System Sciences, 21(2): 1251.

Liang, X., Zhan, H., Zhang, Y.K., Schilling, K., 2017b. Base flow recession from unsaturated-saturated porous media considering lateral unsaturated discharge and aquifer compressibility. Water Resour Res, 53(9): 7832-7852.

Malama, B., 2011. Alternative linearization of watertable kinematic condition for unconfined aquifer pumping test modeling and its implications for specific yield estimates. J. Hydrol. 399, 141-147. DOI: 10.1016/j.jhydrol.2010.11.007.

Malama, B., Kuhlman, K.L., Barrash, W., 2007. Semi-analytical solution for flow in leaky unconfined aquifer-aquitard systems. J. Hydrol. 346, 59-68. DOI: 10.1016/j.jhydrol.2007.08.018.

Malama, B., Kuhlman, K.L., Barrash, W., 2008. Semi-analytical solution for flow in a leaky unconfined aquifer toward a partially penetrating pumping well. J. Hydrol. 356, 234-244. DOI: 10.1016/j.jhydrol.2008.03.029.

Martin, P., Frind, E., 1998. Modeling a complex multi-aquifer system: The Waterloo moraine. Groundwater 36, 679-690. DOI: 10.1111/j.1745-6584.1998.tb02843.x.

Michels, H., 1963. Abscissas and weight coefficients for Lobatto quadrature. Math. Comput. 17, 237-244. DOI: 10.1090/S0025-5718-1963-0158540-4.

Milanovic, P., Aghili, B., 1993. Hydrogeological characteristics and groundwater mismanagement of Kazerun karstic aquifer, Zagros, Iran. In Hydrogeological Processes in Karst Terranes, Gunay, G., Johnson, A.I., Back, W. (Eds.). Proceedings of the International Symposium and Field Seminar, Antalya, Turkey, 7-17 October 1990. International Association of Hydrological Sciences Publication No. 207, pp. 163-171, http://iahs.info/uploads/dms/iahs_207_0163.pdf, last accessed 16 July 2107.

Mishra, P.K., Neuman, S.P., 2010. Improved forward and inverse analyses of saturated-unsaturated flow toward a well in a compressible unconfined aquifer. Water Resour. Res. 46, W07508, 16 pp. DOI: 10.1029/2009WR008899.

Mishra, P.K., Vesselinov, V.V., Kuhlman, K.L., 2012. Saturated-unsaturated flow in a compressible leaky-unconfined aquifer. Adv. Water Resour. 42, 62-70. DOI: 10.1016/j.advwatres.2012.03.007.

Moench, A.F., 1985. Transient flow to a large-diameter well in an aquifer with storative semiconfining layers. Water Resour. Res. 21, 1121-1131. DOI: 10.1029/WR021i008p01121.

Moench, A.F., 1995. Combining the Neuman and Boulton models for flow to a well in an unconfined aquifer. Groundwater 33, 378-384. DOI: 10.1111/j.1745-6584.1995.tb00293.x.

Moench, A.F., 1996. Flow to a well in a water-table aquifer: An improved Laplace transform solution. Groundwater 34, 593-596. DOI: 10.1111/j.1745-6584.1996.tb02045.x.

Moench, A.F., 1997. Flow to a well of finite diameter in a homogeneous, anisotropic watertable aquifer. Water Resour. Res. 33, 1397-1407. DOI: 10.1029/97WR00651.

Moench, A.F., Garabedian, S.P., LeBlanc, D.R., 2000. Estimation of hydraulic parameters from an unconfined aquifer test conducted in a glacial outwash deposit, Cape Cod, Massachusetts. U.S. Dept. of the Interior, U.S. Geological Survey, Open-File Report 2000-485, 132 pp. https://pubs.usgs.gov/of/2000/ofr00-485/pdf/OFR00-485.pdf, last accessed 17 July 2017.

Neuman, S.P., 1972. Theory of flow in unconfined aquifers considering delayed response of the watertable. Water Resour. Res. 8, 1031-1045. DOI: 10.1029/WR008i004p01031.

Neuman, S.P., 1974. Effect of partial penetration on flow in unconfined aquifers considering delayed gravity response. Water Resour. Res. 10, 303-312. DOI: 10.1029/WR010i002p00303.

Neuman, S.P., Witherspoon, P.A., 1969. Theory of flow in a confined two aquifer system. Water Resour. Res. 5, 803-816. DOI: 10.1029/WR005i004p00803.

Park, E., Zhan, H., 2003. Hydraulics of horizontal wells in fractured shallow aquifer systems. J. Hydrol. 281, 147-158. DOI: 10.1016/S0022-1694(03)00206-3.

Parlange, J.Y., Brutsaert, W., 1987. A capillarity correction for free surface flow of groundwater. Water Resour Res, 23(5): 805-808.

Press, W.H., Teukolsky, S.A., Vetterling, W.T., Flannery, B.P., 1992. Numerical recipes in FORTRAN 77, The Art of Scientific Computing, Second Edition, Volume 1 of Fortran Numerical Recipes. Cambridge Univ. Press, Cambridge, United Kingdom. DOI: 10.2277/052143064X.

Samani, N., Sedghi, M.M., 2015. Semi-analytical solutions of groundwater flow in multi-zone (patchy) wedge-shaped aquifers. Adv. Water Resour. 77, 1-16. DOI: 10.1016/j.advwatres.2015.01.003.

Sauter, M., 1990. Double porosity models in karstified limestone aquifers: Field validation and data provision. In Hydrogeological Processes in Karst Terranes, Gunay, G., Johnson, A.I., Back, W. (Eds.). Proceedings of the International Symposium and Field Seminar, Antalya, Turkey, 7-17 October 1990. International Association of Hydrological Sciences Publication No. 207, pp. 261-279. http://hydrologie.org/redbooks/a207/iahs_207_0261.pdf, last accessed 17 July 2017.

Sedghi, M.M., Samani, N., 2010. Three-dimensional semianalytical solutions of groundwater flow to a well in fractured wedge-shaped aquifers. J. Hydrol. Eng. 15, 974-984. DOI: 10.1061/(ASCE)HE.1943-5584.0000269.

Sedghi, M.M., Samani, N., 2015. Semi-analytical solutions for flow to a well in an unconfined-fractured aquifer system. Adv. Water Resour. 83, 89-101. DOI: 10.1016/j.advwatres.2015.05.018.

Sedghi, M.M., Samani, N., Sleep, B., 2009. Three-dimensional semi-analytical solution to groundwater flow in confined and unconfined wedge-shaped aquifers. Adv. Water Resour. 32, 925-935. DOI: 10.1016/j.advwatres.2009.03.004.

Sedghi, M.M., Samani, N., Sleep, B., 2012. Boundary depletion rate and drawdown in leaky wedge-shaped aquifers. Hydrol. Process. 26, 3101-3113. DOI: 10.1002/hyp.8338.

Serra, K., Reynolds, A.C., Raghavan, R., 1983. New pressure transient analysis methods for naturally fractured reservoirs. J. Petrol. Tech. 35, 2271-2283. DOI: 10.2118/10780-PA.

Streltsova, T., 1976. Hydrodynamics of groundwater flow in a fractured formation. Water Resour. Res. 12, 405-414. DOI: 10.1029/WR012i003p00405.

Subyani, A.M., 2004. Use of chloride-mass balance and environmental isotopes for evaluation of groundwater recharge in the alluvial aquifer, Wadi Tharad, western Saudi Arabia. Env. Geol. 46, 741-749. DOI:10.1007/s00254-004-1096-y.

Sun, D., Zhan. H., 2006. Flow to a horizontal well in an aquitard-aquifer system. J. Hydrol. 321, 364-376. DOI: 10.1016/j.jhydrol.2005.08.008.

Tartakovsky, G.D., Neuman, S.P., 2007. Three-dimensional saturated-unsaturated flow with axial symmetry to a partially penetrating well in a compressible unconfined aquifer. Water Resour. Res. 43. DOI: 10.1029/2006WR005153.

Veling, E.J.M, Maas, C., 2009. Strategy for solving semi-analytically three-dimensional transient flow in a coupled N-layer aquifer system. J. Eng. Math. 64, 145-161. DOI: 10.1007/s10665-008-9256-9.

Wagner, W., 2011. Groundwater in the Arab Middle East. Springer, New York USA.

Warren, J., Root, P.J., 1963. The behavior of naturally fractured reservoirs. Soc. Petrol. Eng. J. 3, 245-255. DOI: 10.2118/426-PA.

Zhan, H., Park, E., 2003. Horizontal well hydraulics in leaky aquifers. J. Hydrol. 281, 129-146. DOI: 10.1016/S0022-1694(03)00205-1.

Zhan, H., Zlotnik, V.A., 2002. Groundwater flow to a horizontal or slanted well in an unconfined aquifer. Water Resour. Res. 38, 13-1–13-11. DOI: 10.1029/2001WR000401.

Figure Captions

Figure 1. Schematic cross section of an unconfined-fractured aquifer system separated by an aquitard: (a) Pumped well screened in the unconfined aquifer. (b) Pumped well screened in the fractured aquifer. Variables pertaining to each region of the aquifer are defined in the text.

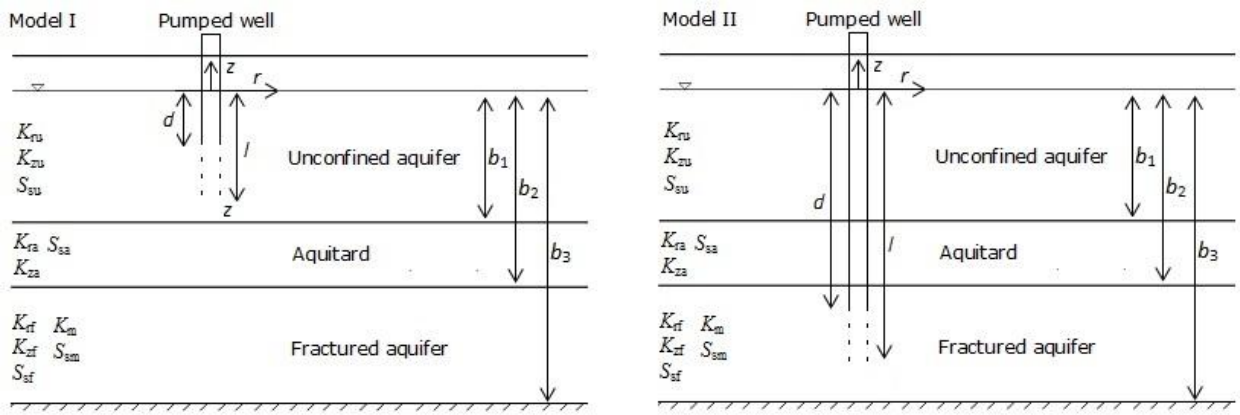

Figure 2. Dimensionless drawdown in the three-layer aquifer system for different values of K_{rf}/K_{ru}. The pumping well is screened in the unconfined aquifer (Fig. 1a).

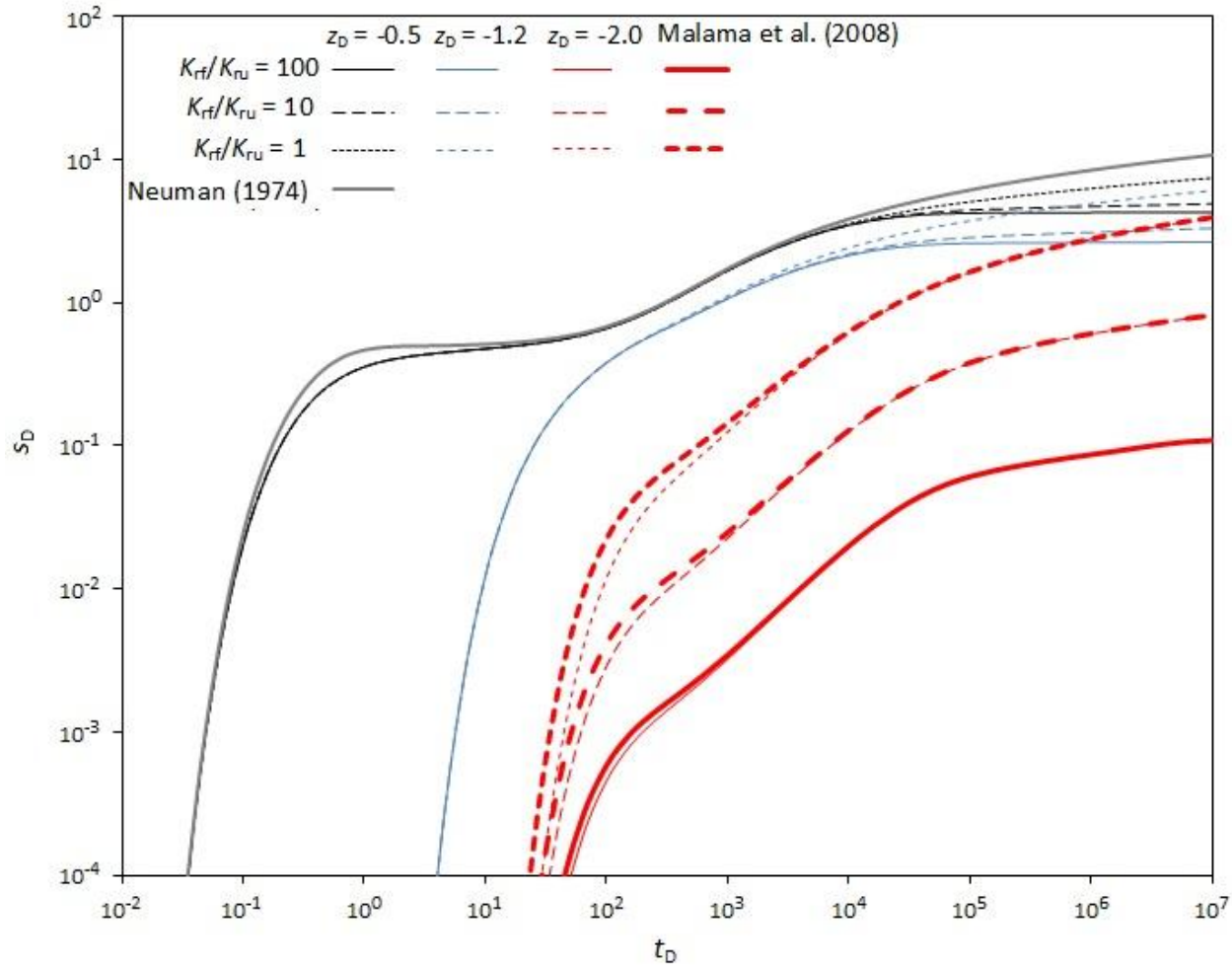

Figure 3. Dimensionless drawdown in the three-layer aquifer system for different values of K_{zf}/K_{zu}. The pumping well is screened in the unconfined aquifer.

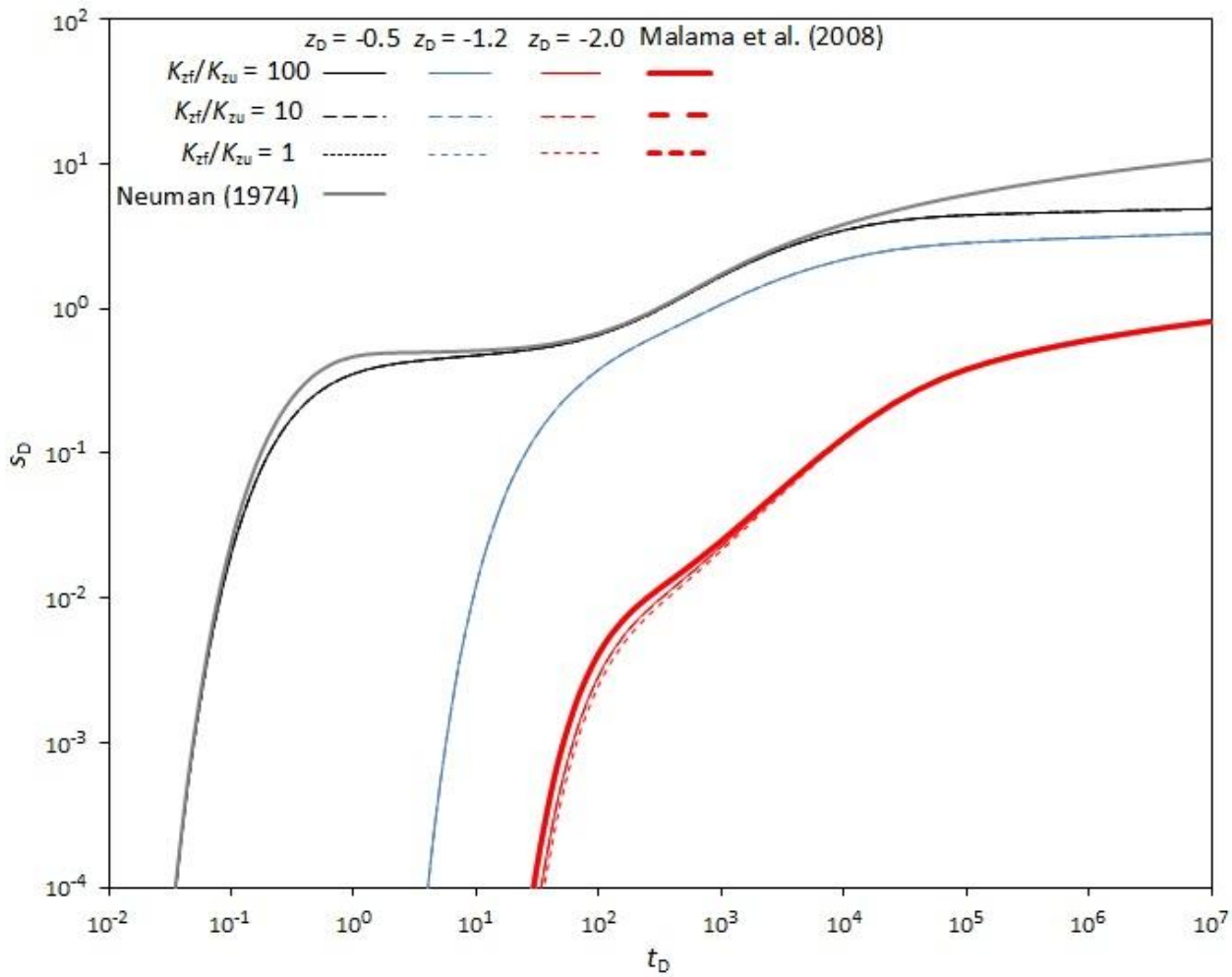

Figure 4. Dimensionless drawdown in the three layer-aquifer system for different values of K_{rf}/K_m. The pumping well is screened in the unconfined aquifer.

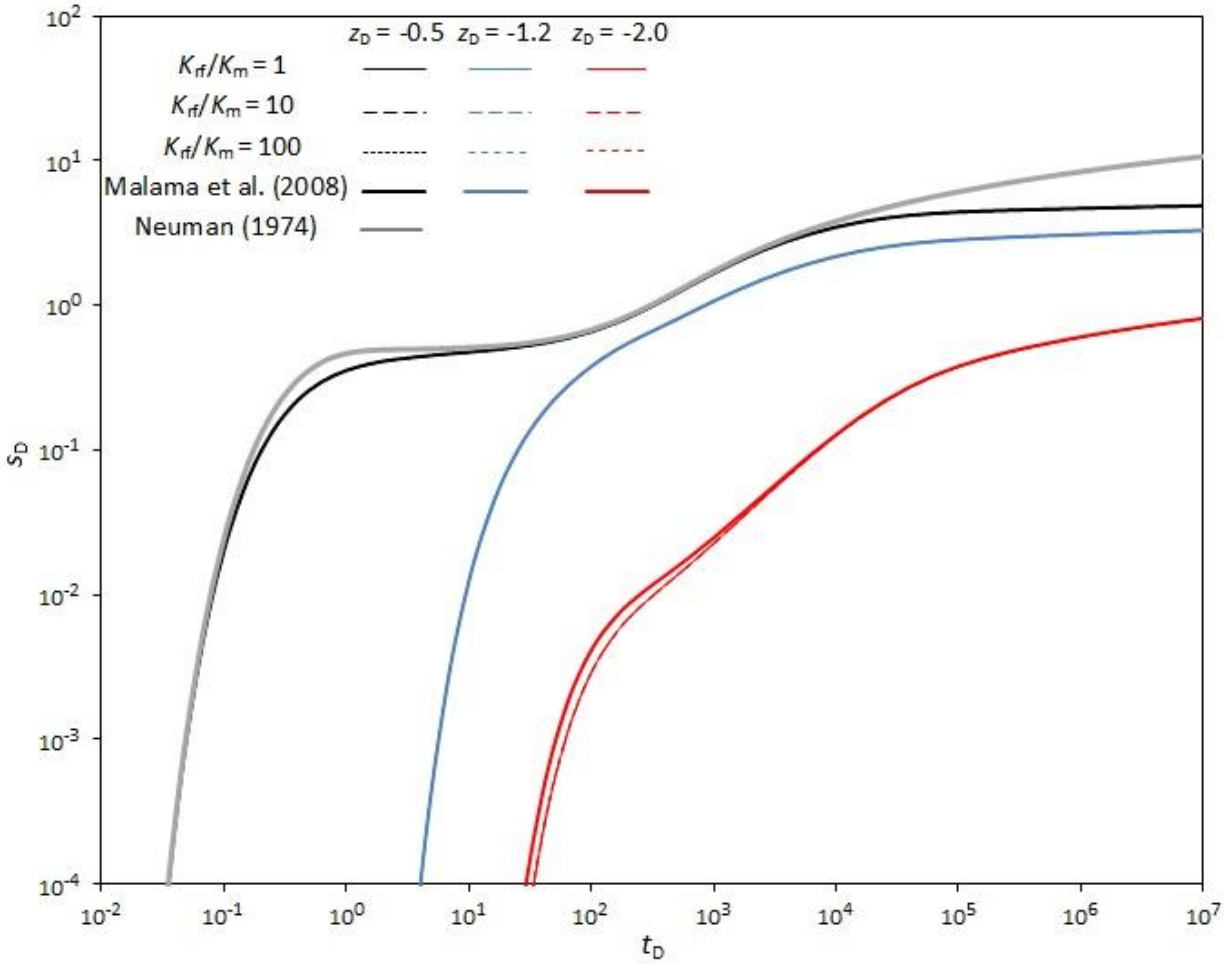

Figure 5. Effects of S_{sm}/S_{mf} on the dimensionless drawdown in the aquifer system. The pumping well is screened in the unconfined aquifer.

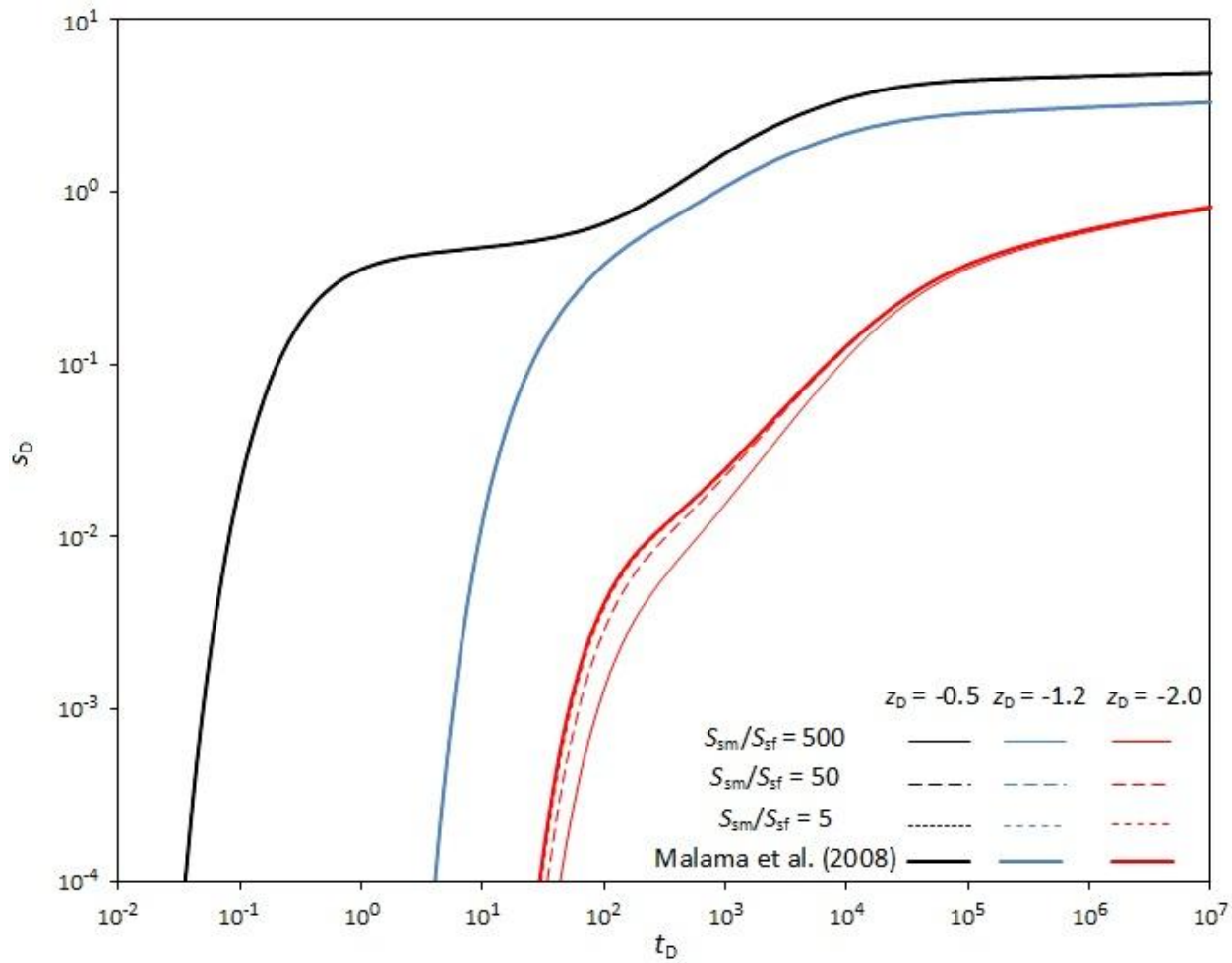

Figure 6. Effects of S_y on the dimensionless drawdown in the aquifer system. The pumping well is screened in the unconfined aquifer.

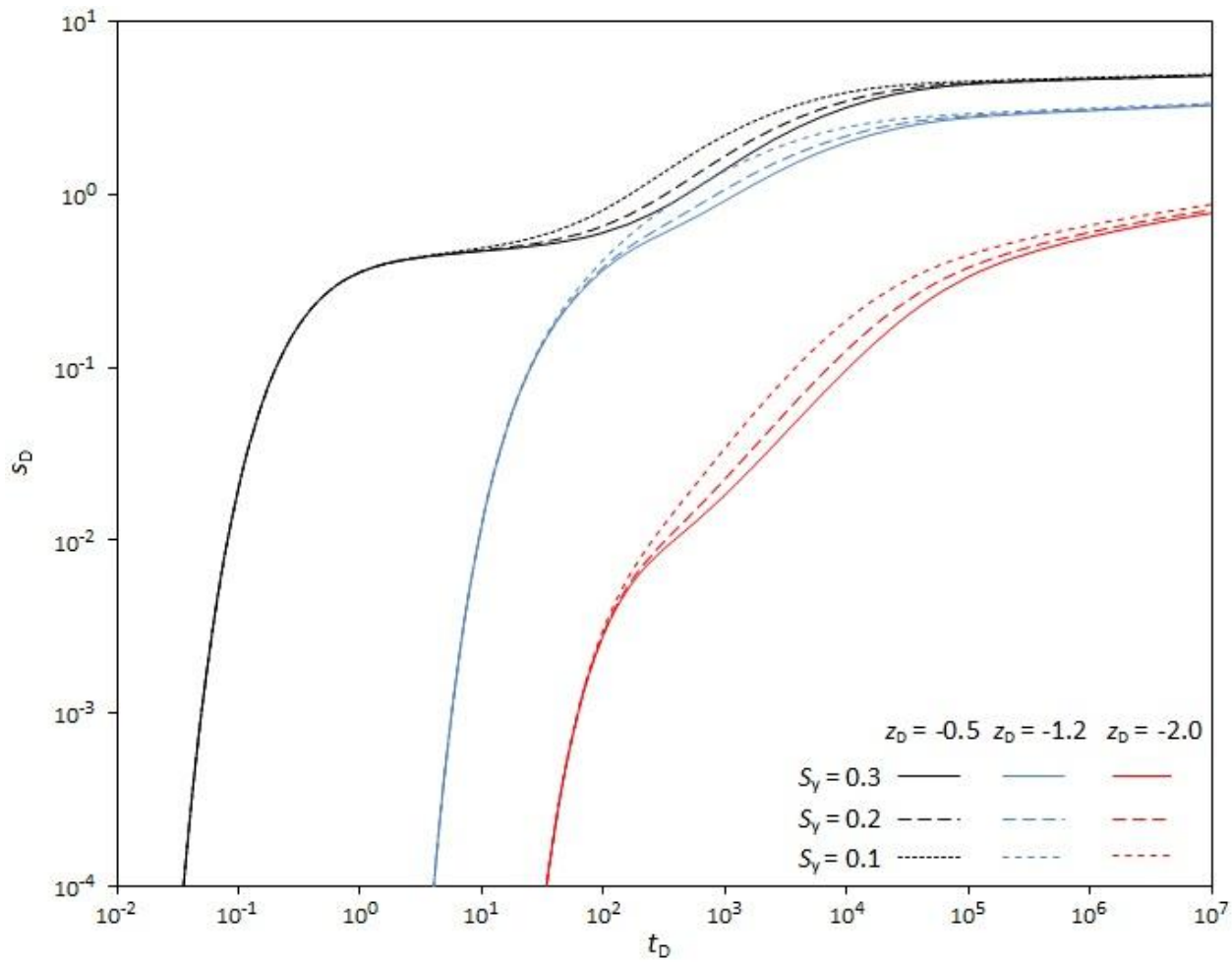

Figure 7. Effects of β_D on the dimensionless drawdown in the aquifer system. The pumping well is screened in the unconfined aquifer.

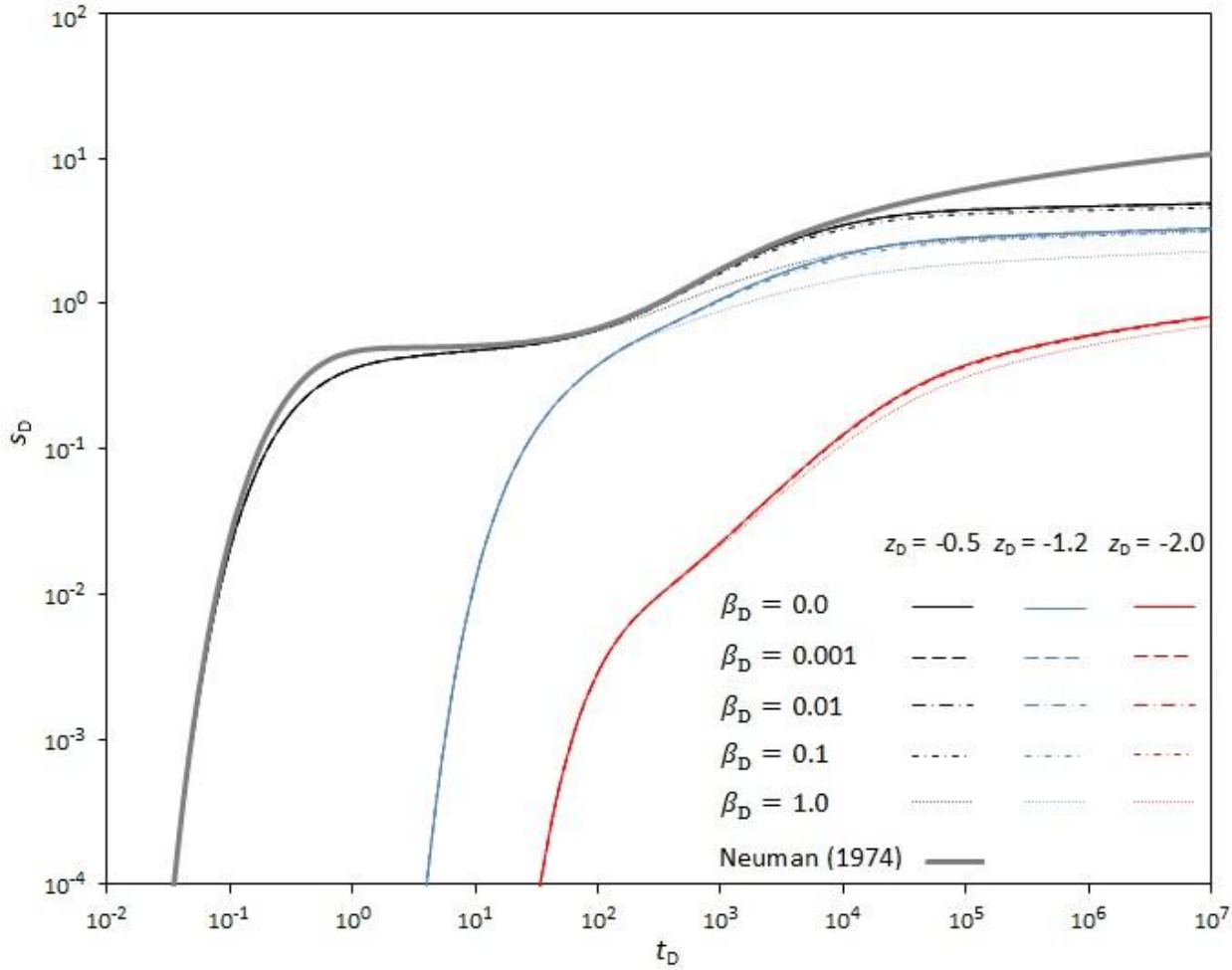

Figure 8. Dimensionless drawdown in the three-layer aquifer system for different values of K_{rf}/K_{ru}. The pumping well is screened in the fractured aquifer.

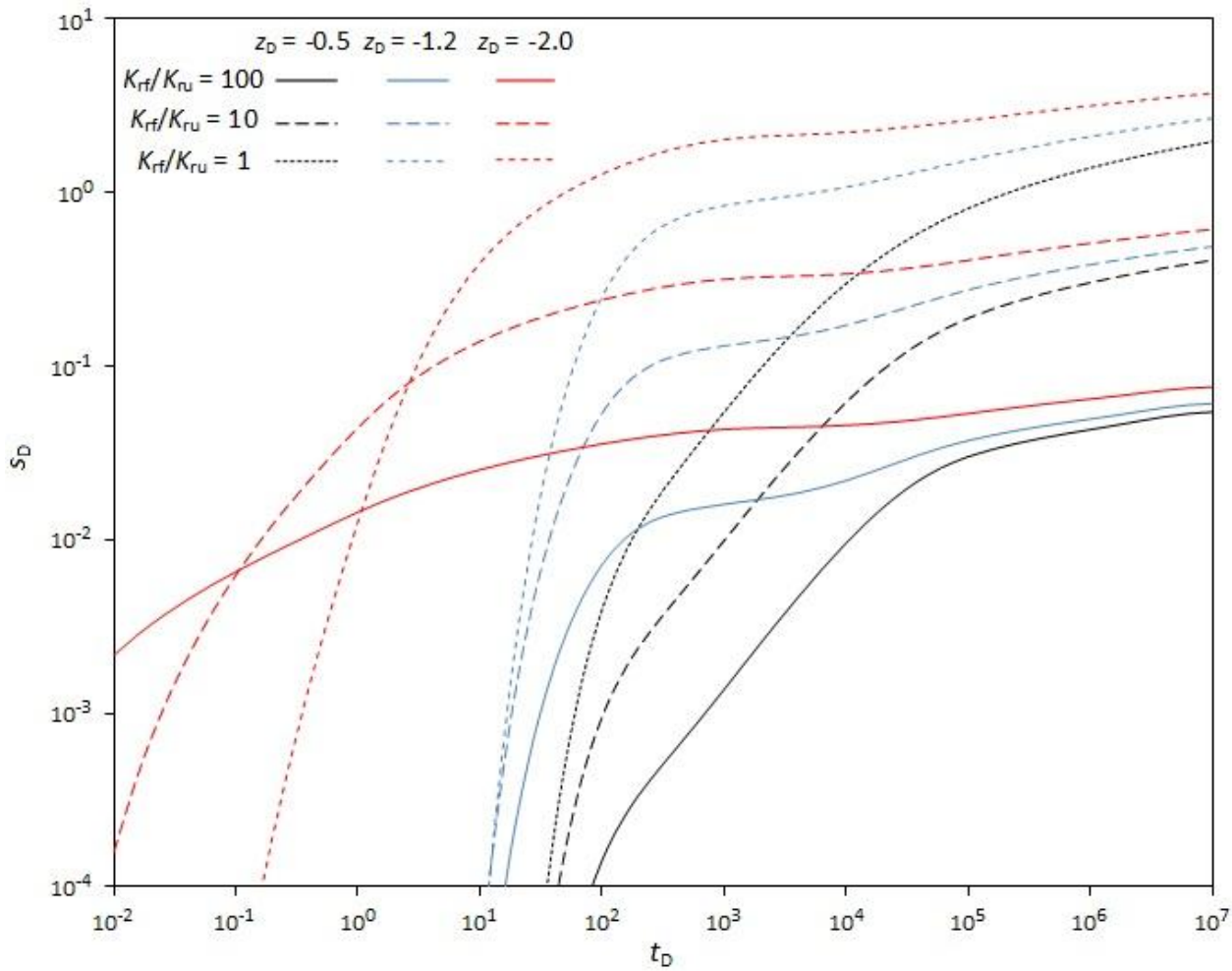

Figure 9. Dimensionless drawdown in the three-layer aquifer system for different values of K_{zf}/K_{zu}. The pumping well is screened in the fractured aquifer.

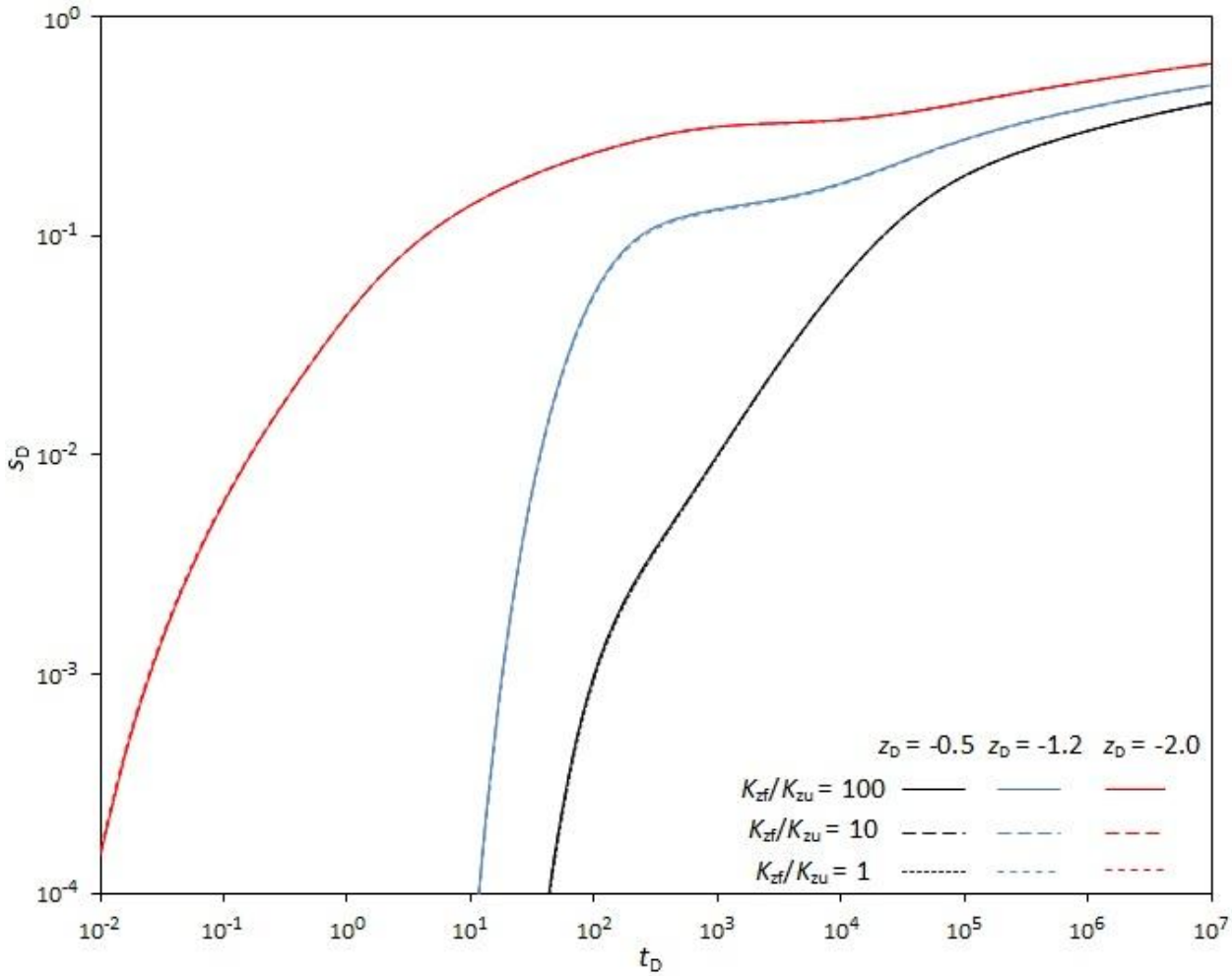

Figure 10. Effects of K_{rf}/K_m on the dimensionless drawdown in the aquifer system. The pumping well is screened in the fractured aquifer.

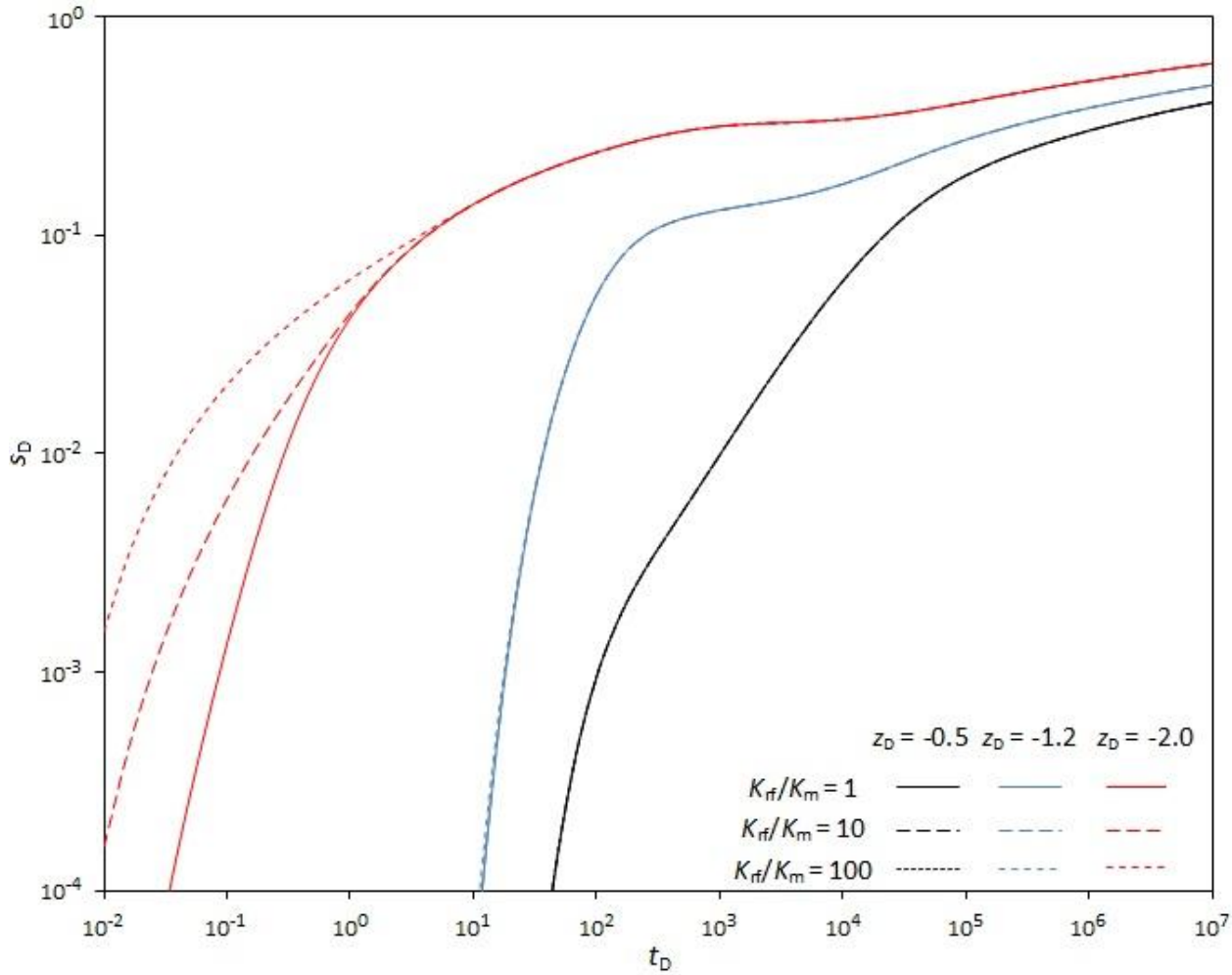

Figure 11. Effects of S_y on the dimensionless drawdown in the aquifer system. The pumping well is screened in the fractured aquifer.

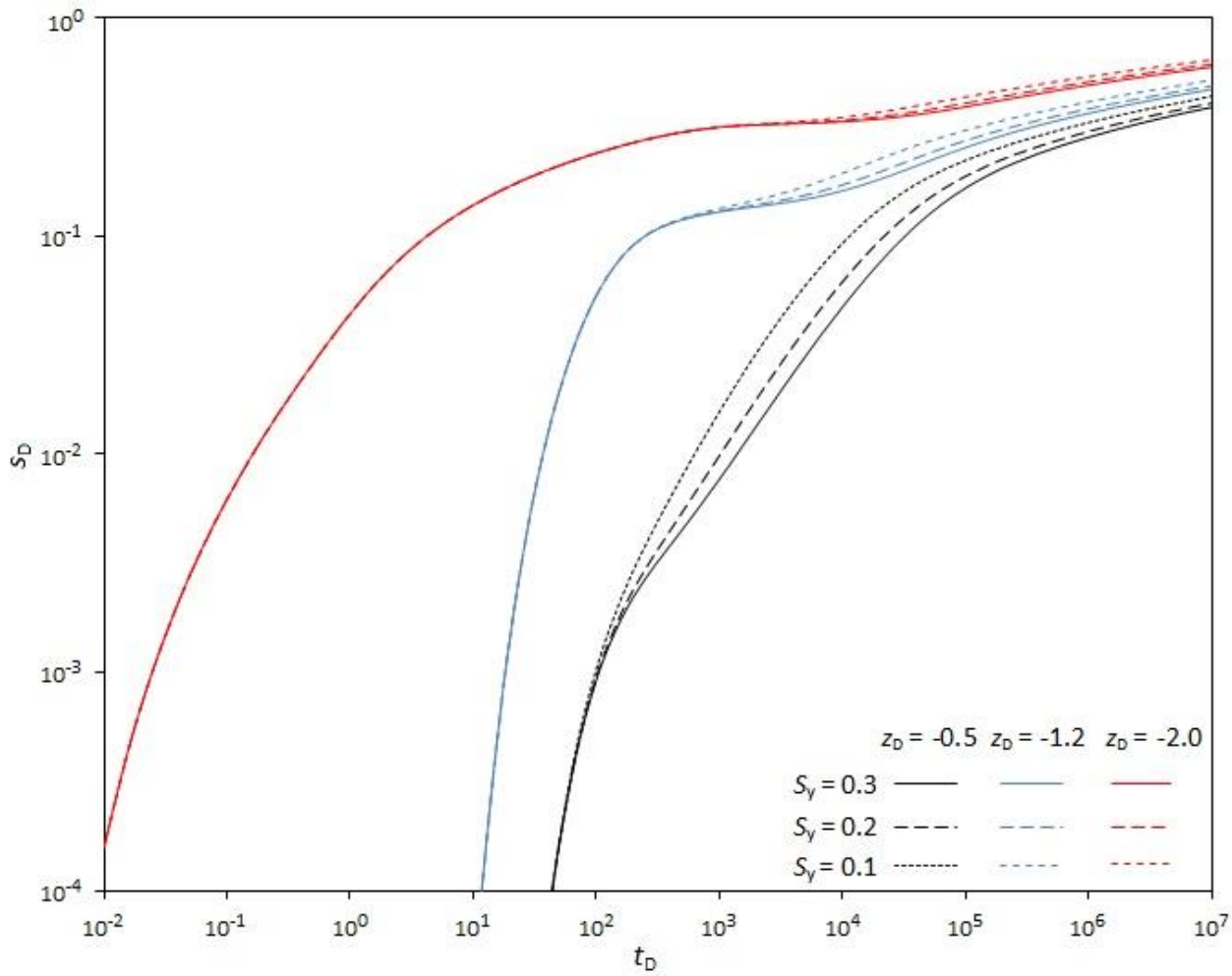

Figure 12. Effects of S_{sm}/S_{mf} on the dimensionless drawdown in the aquifer system. The pumping well is screened in the fractured aquifer.

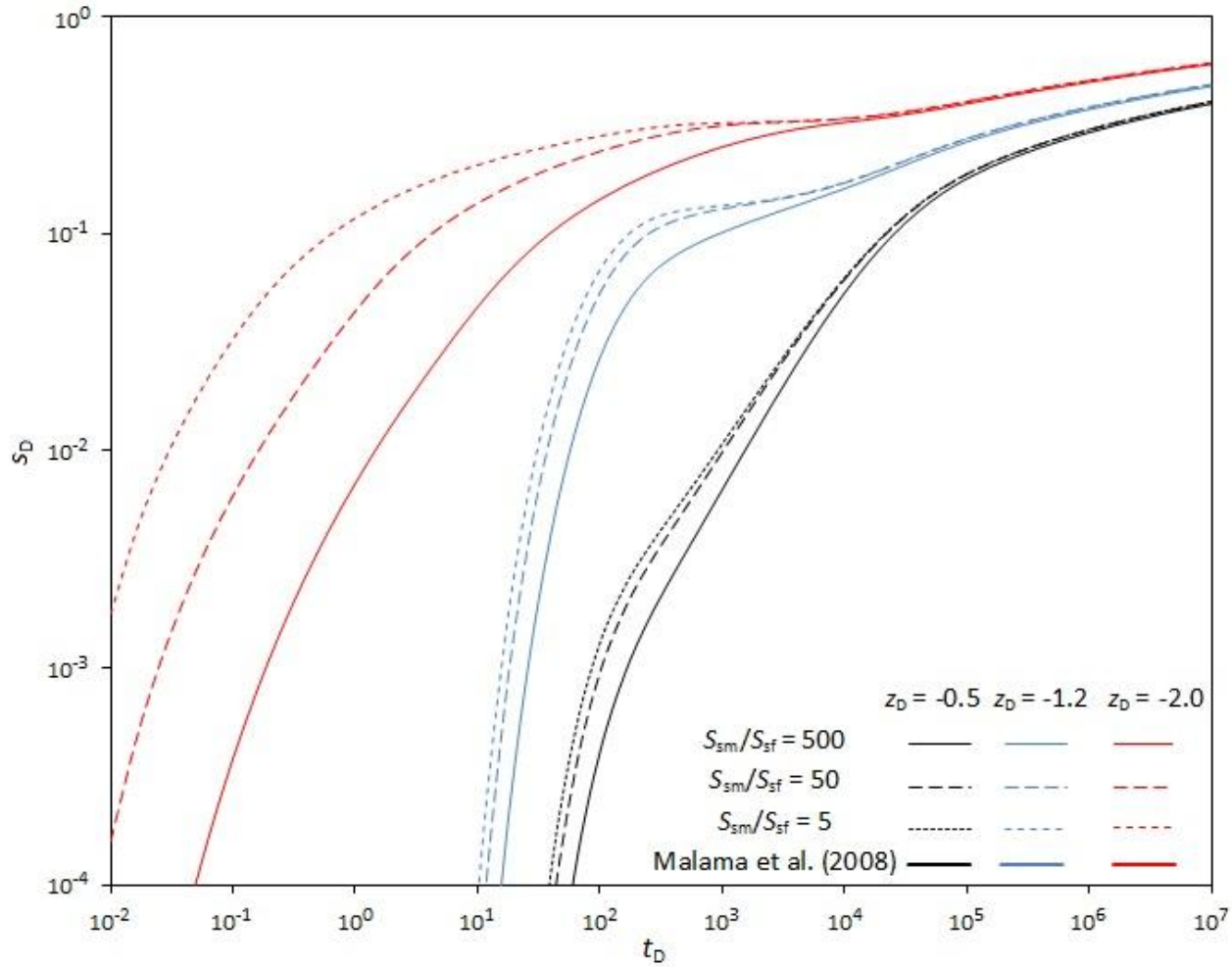

Figure 13. Effects of β_D on the dimensionless drawdown in the aquifer system. The pumping well is screened in the fractured aquifer.

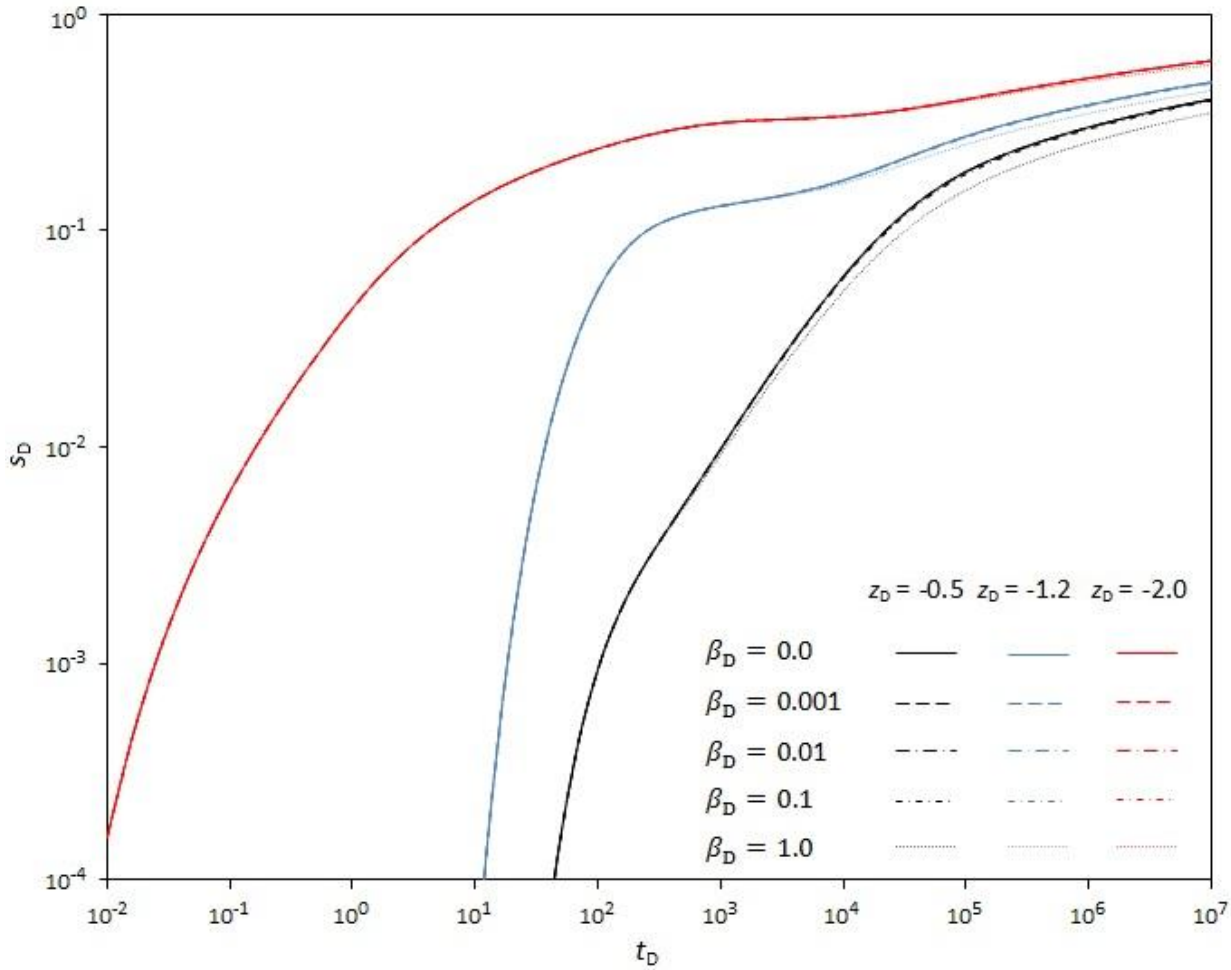

Table 1. Dimensionless variables.

$s_{uD} = \dfrac{s_u}{Q/(4\pi b_1 K_{ru})}$	$d_D = \dfrac{d}{b_1}$	$\beta_D = \dfrac{\beta}{b_1}$
$s_{aD} = \dfrac{s_a}{Q/(4\pi b_1 K_{ru})}$	$\tilde{r}_{Dm} = \dfrac{\tilde{r}_m}{b_1}$	$\xi = \dfrac{\eta_u \alpha_{Dy}}{p}$
$s_{fD} = \dfrac{s_f}{Q/(4\pi b_1 K_{ru})}$	$t_D = \dfrac{K_{ru}}{S_{su} b_1^2} t$	$\gamma_1 = \dfrac{\eta_a}{\eta_u} \dfrac{K_{za}}{K_{zu}}$

$$s_{\mathrm{mD}} = \frac{s_{\mathrm{m}}}{Q/(4\pi b_1 K_{\mathrm{ru}})} \qquad \alpha_{\mathrm{Dz}}^{\mathrm{u}} = \frac{\alpha_{\mathrm{zu}}}{\alpha_{\mathrm{ru}}} \qquad \gamma_2 = \frac{\eta_{\mathrm{f}}}{\eta_{\mathrm{a}}}\frac{K_{\mathrm{zf}}}{K_{\mathrm{za}}}$$

$$z_{\mathrm{D}} = \frac{z}{b_1} \qquad \alpha_{\mathrm{Dz}}^{\mathrm{a}} = \frac{\alpha_{\mathrm{za}}}{\alpha_{\mathrm{ru}}} \qquad \omega = \frac{K_{\mathrm{m}} S_{\mathrm{su}}}{K_{\mathrm{ru}} S_{\mathrm{m}}}$$

$$r_{\mathrm{D}} = \frac{r}{b_1} \qquad \alpha_{\mathrm{Dz}}^{\mathrm{f}} = \frac{\alpha_{\mathrm{zf}}}{\alpha_{\mathrm{ru}}} \qquad \gamma = \frac{3K_{\mathrm{m}}}{\tilde{r}_{\mathrm{Dm}} K_{\mathrm{ru}}}\left[\sqrt{\frac{p}{\omega}}\coth\left(\sqrt{\frac{p}{\omega}}\tilde{r}_{\mathrm{Dm}}\right) - \frac{1}{\tilde{r}_{\mathrm{Dm}}}\right]$$

$$b_{2\mathrm{D}} = \frac{b_2}{b_1} \qquad \alpha_{\mathrm{Dr}}^{\mathrm{a}} = \frac{\alpha_{\mathrm{ra}}}{\alpha_{\mathrm{ru}}} \qquad \eta_{\mathrm{u}} = \sqrt{\frac{p + a^2}{\alpha_{\mathrm{Dz}}^{\mathrm{u}}}}$$

$$b_{3\mathrm{D}} = \frac{b_3}{b_1} \qquad \alpha_{\mathrm{Dr}}^{\mathrm{f}} = \frac{\alpha_{\mathrm{rf}}}{\alpha_{\mathrm{ru}}} \qquad \eta_{\mathrm{a}} = \sqrt{\frac{p + \alpha_{\mathrm{Dr}}^{\mathrm{a}} a^2}{\alpha_{\mathrm{Dz}}^{\mathrm{a}}}}$$

$$l_{\mathrm{D}} = \frac{l}{b_1} \qquad \alpha_{\mathrm{Dy}} = \frac{\alpha_{\mathrm{y}}}{\alpha_{\mathrm{ru}}} \qquad \eta_{\mathrm{f}} = \sqrt{\frac{p + \alpha_{\mathrm{Dr}}^{\mathrm{f}} a^2}{\alpha_{\mathrm{Dz}}^{\mathrm{f}}}}$$

Table 2. Default parameter ratios.

Parameter	Value	Parameter	Value
r_{D}	1	$\tilde{r}_{\mathrm{mD}}$	0.1
$b_{2\mathrm{D}}$	1.5	$b_{3\mathrm{D}}$	2.5
d_{D}	0.5 (Model I)	l_{D}	1.0 (Model I)
d_{D}	2.0 (Model II)	d_{D}	2.5 (Model II)
$\frac{K_{\mathrm{rf}}}{K_{\mathrm{ru}}}$	10	$\frac{K_{\mathrm{zf}}}{K_{\mathrm{zu}}}$	10

$\frac{K_{\mathrm{rf}}}{K_{\mathrm{m}}}$	10^2	$\frac{S_{\mathrm{sm}}}{S_{\mathrm{sf}}}$	5.0×10^2
β_{D}	0	$\alpha_{\mathrm{Dz}}^{\mathrm{u}}$	1.0
$\alpha_{\mathrm{Dz}}^{\mathrm{a}}$	4.0×10^{-4}	$\alpha_{\mathrm{Dz}}^{\mathrm{f}}$	20.0
$\alpha_{\mathrm{Dr}}^{\mathrm{a}}$	4.0×10^{-4}	$\alpha_{\mathrm{Dr}}^{\mathrm{f}}$	20.0
α_{Dy}	2.0×10^{-3}		

- The Laplace-Hankel domain solutions of flow in a three-layer aquifer system obtained.
- The aquifer system consists of an unconfined-fractured aquifer separated by an aquitard.
- The pumping well screened in the overlying unconfined or underlying fractured aquifer.
- Solutions are presented in form of dimensionless time-drawdown curves.
- The effect of hydraulic parameters of each layer on the three-layer aquifer system is explored.